DOT/FAA/AR-05/42

Office of Aviation Research
Washington, D.C. 20591

Computational Study of Large Droplet Breakup in the Vicinity of an Airfoil

October 2005

Final Report

This document is available to the U.S. public through the National Technical Information Service (NTIS), Springfield, Virginia 22161.

U.S. Department of Transportation
Federal Aviation Administration

NOTICE

Technical Report Documentation Page

1. Report No.	2. Government Accession No.	3. Recipient's Catalog No.
DOT/FAA/AR-05/42		

4. Title and Subtitle	5. Report Date
COMPUTATIONAL STUDY OF LARGE DROPLET BREAKUP IN THE VICINITY OF AN AIRFOIL	October 2005
	6. Performing Organization Code

7. Author(s)	8. Performing Organization Report No.
J. Tan, M. Papadakis, and M. K. Sampath	

9. Performing Organization Name and Address	10. Work Unit No. (TRAIS)
Department of Aerospace Engineering Wichita State University Wichita, KS 67260	11. Contract or Grant No.

12. Sponsoring Agency Name and Address	13. Type of Report and Period Covered
U.S. Department of Transportation Federal Aviation Administration Office of Aviation Research Washington, DC 20591	Final Report
	14. Sponsoring Agency Code AIR-100

15. Supplementary Notes

The Federal Aviation Administration Airport and Aircraft Safety R&D Division Technical Monitor was Manuel Rios.

16. Abstract

A study was conducted to assess the effects of aerodynamic forces on the behavior of water droplets traversing near an airfoil. The analysis was performed using the Taylor Analogy Breakup (TAB) model, which can simulate droplet oscillation and distortion. In general, the TAB model is capable of modeling droplet breakup with an acceptable level of accuracy, but its application is limited to vibrational and bag breakup modes only. The model does not rely on a unique critical value (e.g., Weber number of 13.0) to determine breakup. Instead, droplet breakup occurs when the lateral radius of the distorted droplet exceeds the half-radius of an undisturbed droplet. Although the actual breakup modes near an airfoil are unknown, it is believed that the validations of the TAB model with the experimental data collated from investigations conducted with horizontal and vertical tunnels were appropriate for assessing droplet breakup near the airfoil because the flow fields in these tunnels were similar to those found near the airfoils used in the present study. Before the parametric droplet breakup studies, the sensitivity of droplet breakup to the resolution of the computational mesh and the initial droplet release location was assessed. The findings from this sensitivity study were used in the computation of droplet breakup in the flow field of the following two-dimensional airfoils: two NACA0012 airfoils with chord lengths of 3 and 20 ft and a three-element, high-lift airfoil with chord length of 20 ft. Water droplets with diameters of 100, 500, and 1000 μm were released at about 5 chords upstream of each airfoil. The simulations showed that breakup generally occurred in regions with severe pressure gradient. It was also found that droplets that broke up near a wall surface did not have sufficient time to completely disintegrate before hitting the wall. This was the case with droplet diameters of 500 and 1000 μm near the leading edge of the 20-ft chord NACA0012 airfoil and the leading edges of the slat and flap elements of the high-lift airfoil.

17. Key Words	18. Distribution Statement
Supercooled large droplets in-flight icing, Weber number, Rabin number, Taylor Analogy Breakup Model, Bond number	This document is available to the public through the National Technical Information Service (NTIS) Springfield, Virginia 22161.

19. Security Classif. (of this report)	20. Security Classif. (of this page)	21. No. of Pages	22. Price
Unclassified	Unclassified	72	

ACKNOWLEDGEMENTS

This work was supported by a grant from the Federal Aviation Administration (FAA) under the Airworthiness Assurance Center of Excellence. The authors would like to thank Mr. Manny Rios and Dr. James T. Riley of the FAA William J. Hughes Technical Center; Mr. Eugene Hill, the FAA Icing National Resource Specialist; and Tom Bond, Chief of the Icing Branch at the NASA Glenn Research Center, for their support.

TABLE OF CONTENT

LIST OF FIGURES

LIST OF TABLES

LIST OF ACRONYMS

2D	Two-dimensional
AOA	Angle of attack
Bo	Bond number
CFD	Computational fluid dynamics
La	Laplace number
LE	Leading edge
Oh	Ohnesorge number
Ra	Rabin number
Re	Reynolds number
SLD	Supercooled large droplet
TAB	Taylor Analog Breakup
TE	Trailing edge
We	Weber number

EXECUTIVE SUMMARY

A literature review of droplet breakup and two-dimensional simulations of small and large droplet breakup in the proximity of airfoils were performed in support of future research to develop experimental data and simulation tools for aircraft icing applications.

A survey of the published literatures showed that droplet breakup can be simulated using numerical and empirical methods. It also showed that nondimensional parameters such the Weber, Rabin, and Bond numbers can be used to characterize droplet breakup. The breakup criteria and breakup mode depend on the flow and droplet conditions, e.g., relative droplet-gas velocity, severity of pressure gradients, droplet diameter, etc. Numerical droplet breakup models were also found in the published literature, including the Taylor Analogy Breakup (TAB) and Reitz models. Preliminary computations were performed with a commercial computational fluid dynamics code to assess the suitability of these two models for simulating droplet breakup. Theses studies led to the selection of the TAB model for the large droplet breakup studies in the proximity of airfoils.

Validation of the TAB model was performed by comparing predicted critical breakup values with published experimental data collated from vertical and horizontal wind tunnel experiments. The results showed that the TAB model is capable of simulating critical breakup conditions (such as droplet diameter and velocity prior to breakup) with acceptable level of accuracy. However, the model is limited to vibrational and bag types of breakup only. Computations were performed to assess the sensitivity of droplet breakup to the grid resolution and initial droplet release locations (from the airfoil). The effects of the airfoil chord length and droplet size on droplet breakup behavior were assessed using NACA0012 airfoils with 3-ft and 20-ft chord lengths. The droplet sizes used in the simulation studies were 100, 500, and 1000 μm, representing the maximum droplet diameter in a Title 14 Code of Federal Regulations Part 25, Appendix C cloud, threshold size for freezing drizzle and rain, respectively. A 20-ft chord three-element airfoil that was representative of large modern transport wing section was also used in the simulations to explore droplet breakup in the proximity of high-lift systems. The slat and flap of this airfoil were set to 30° leading edge (LE) and trailing edge (TE) down, respectively, to simulate a landing configuration.

The results obtained from the two-dimensional simulations of droplet breakup near the small and large NACA0012 airfoils and three-element high-lift-system indicated the following:

- Droplet breakup occurred mainly in areas with severe pressure gradients, such as the LE stagnation region and the high- and low-pressure regions near the leading and trailing edges of the airfoils investigated.

- There were more occurrences of droplet breakup in the three-element airfoil (angle of attack (AOA) = 0°) compared to the NACA0012 airfoil (AOA = 0°) for the same droplet size and chord length.

- Whenever droplet breakup occurred close to the airfoil surface, e.g., LE stagnation region, there was insufficient distance between the wall and the location where droplet

breakup was initiated for the fragmented droplets to achieve complete breakup prior to their impingement on the wall.

- The droplet breakup characteristics obtained with the two NACA0012 airfoils showed that droplet breakup in the case of the 3-ft chord airfoil occurred aft of the LE, whereas for the 20-ft chord airfoil, it occurred near the stagnation region only.

- Larger droplets were more susceptible to droplet breakup than smaller droplets when subjected to similar aerodynamic forces.

- Aerodynamic forces had a significant effect on the trajectories of the small droplets. The trajectories of the larger droplets (≥ 500 μm) were generally 'ballistic' in nature.

It must be noted that for the current study the breakup modes that were simulated with the TAB model were limited to vibrational and bag modes. Extensive experimental and computational studies are needed before general statements regarding the effects of droplet breakup on the impingement and icing characteristics of aerodynamic surfaces can be made.

1. INTRODUCTION.

It has been reported by some aircraft manufacturers that large water droplets tend to breakup near wing surfaces when flying into inclement weather conditions. These reports were based on visual observations from pilots operating large transport aircraft. It is not known whether general transport and other smaller aircraft operators have made similar observations. However, research into fuel atomization has shown that droplets can break up when subjected to severe pressure gradients. Since aircraft also have regions of high and low pressure, e.g., leading edges (LE) of wing, vertical and horizontal stabilizers, etc., it is possible for breakup to occur when droplets traverse across these regions. Droplet breakup can be characterized by the ratio of the aerodynamic forces to the surface tension of a droplet (or better known as Weber number). Large water droplets have relatively weaker surface tension forces compared to the aerodynamic forces, hence, higher Weber number and an increased likelihood of breakup.

Recent in-flight measurements of the droplet spectra in icing clouds (e.g., CFDE-I, CFDE-III, FIRE.ACE, AIRS) conducted by the Federal Aviation Administration, National Aeronautics and Space Administration Glenn Research Center, Meteorological Service of Canada, and the National Research Council of Canada, [1] had shown that supercooled large droplet (SLD) clouds generally exhibit bimodal droplet size distributions. The droplet sizes measured in these clouds ranged from 50 to 3000 μm, which are much larger than those found in Title 14 Code of Federal Regulations Part 25, Appendix C clouds. SLDs are normally associated with freezing drizzle and rain, therefore, droplet breakup may be more commonplace in practice than anticipated. However, it is not known whether droplet breakup affects the ice accretion process due to the lack of experimental data (at the time of writing this report). In addition, current icing codes such as LEWICE and TRAJICE United Kingdom do not include droplet breakup modeling since their applications are mainly for 14 CFR Part 25, Appendix C icing clouds where droplet sizes are small (hence, smaller Weber numbers), therefore, breakup is less likely to occur. With the imminent introduction of new regulations governing SLD icing, it would be prudent to ascertain the effects of droplet breakup on icing and simulations from current generation ice accretion codes.

However, SLD research is still in the embryonic stage; therefore, a preliminary effort was carried out initially to assess the droplet dynamics near airfoils by applying existing numerical techniques to simulate droplet distortion and breakup. The analyses were performed with three droplet sizes and two different airfoil shapes and chord lengths. Single- and multielement airfoils (e.g., with slat and flap elements) were also considered. This report presents the results of the analyses, including limited validation of the Taylor Analog Breakup (TAB) droplet breakup model, which was selected for this study. The features and limitations of this model were also presented, including a review of past and present published literatures on the critical droplet breakup values.

2. OBJECTIVES.

The objective of this study was to assess the potential for droplet breakup to occur in the proximity of an airfoil and to determine the parameters that influence the breakup process prior to the impact with the airfoil. The effects of airfoil size, droplet size, droplet release location, and grid resolution on the breakup process were also investigated.

3. LITERATURE REVIEW ON DROPLET BREAKUP.

There are a large number of published reports on droplet breakup; however, most of these reports are related to aerosol atomization, fuel injection, liquid propellants, and nozzle spray systems. Droplets in these cases are often subjected to very sudden changes in flow conditions, and the facilities commonly used to simulate these flow conditions include shock tubes and horizontal wind tunnels (injection of droplets normal to the flow). In contrast, very few experiments have been conducted in an environment where droplets are subjected to more gradual decelerating or accelerating flows, a condition more likely to be encountered by droplets traveling near an airfoil. The review is, therefore, biased towards the former type of test facilities where a considerable amount of data has been gathered on the physical mechanisms involved in droplet breakup, including formulations of the breakup time and size of the fragmented droplets. A list of the nondimensional groups commonly used to characterize droplet breakup such as Weber (We), Rabin (Ra), Laplace (La), Bond (Bo), and Ohnesorge (Oh) numbers are found in appendix A.

Lane [2-4] was among the early researchers who studied droplet behavior under steady and transient gas flows. He showed that a single drop subjected to a steady stream of air would initially flatten into a disk (also known as an oblate ellipsoid), and at the critical air velocity, it would be blown out into the form of a hollow bag attached to a circular rim. The bursting of this bag produced a fine shower of droplets, but the rim, which contained about 70% of the mass of the original drop, broke up into much larger drops. This breakup process is known as the bag breakup mode (figure B-1 in appendix B). Lane developed the following relation for determining imminent droplet breakup:

$$(u - v)^2 d = 0.612$$

where, u is the critical air velocity (m/s), v is the droplet velocity at the instant of breaking (m/s), and d is the droplet diameter (m). He also discovered that droplets that were subjected to transient gas flows (e.g., air blast from shock waves) exhibited a different breakup mode known as shear or stripping breakup (figure B-1). In this case, the droplet deformed in the opposite direction to that of the bag breakup and formed a convex surface to the flow. The edges of the saucer shape were drawn out into a thin sheet and then into fine filaments, which in turn shed into droplets. He related the critical air velocity to those measured in a steady gas with the following relationship:

$$\frac{Velocity\ \ for\ bursting\ by\ suddenly\ applied\ blast}{Velocity\ \ for\ bursting\ in\ steady\ stream} \approx 0.71$$

Hinze [5 and 6] showed that increasing droplet viscosity could delay the onset of breakup, and in highly viscous fluids, incomplete breakup was observed. He later proposed, using nondimensional groups such as Weber and Ohnesorge numbers (appendix A), to characterize the breakup process. He estimated that the critical Weber number for breakup was approximately 13 for shock flows, and approximately 22 for falling droplets. He also found that the breakup process consisted of several stages, including extreme droplet flattening, formation of a torus with an attached hollow bag-shaped film, and bursting of the film.

Wolfe and Andersen [7] conducted a thorough investigation into the mechanism of droplet breakup and developed equations for the droplet fragment size and breakup time, which until recently, had not been studied by previous researchers. Their experimental tests were conducted in a shock tube with droplets consisting of fluids having a range of viscosities and surface tensions. The tests included a range of droplet sizes and droplet relative velocities with respect to the gas. They explained that shearing of a droplet would occur if the nonuniform pressures exerted on the droplet by the gas flow were sufficient to overcome the surface tension of the liquid. They also suggested that the total drag exerted on a droplet was composed of two components: pressure drag resulting from the pressure distribution over the surface of the droplet, and friction drag resulting from the viscous shear forces at the surface of the droplet. They proposed the following equation for predicting the droplet breakup time:

$$t = \frac{D}{\sqrt{\frac{256\,\mu_d^2}{\rho_d^2 D^2} + \frac{2P}{\rho_d}} - \frac{16\,\mu_d}{\rho_d D}}$$

$$P = \left[\frac{1}{2}\rho_g V_r^2 - 2\frac{\sigma}{D}\right]$$

They also showed that the droplet (fragment) sizes after breakup could be estimated with the following equation:

$$D_{30} = \left[\frac{136\,\mu_d \sigma_d^{1.5} D_0^{0.5}}{\rho_g^2 \rho_d^{0.5} \left|V_d - V_g\right|^4}\right]^{1/3}$$

They also attempted to quantify the drag coefficient (C_D) of the deforming droplets from their experimental data but large uncertainties in the calculated values were found due to the changes in the acceleration of the droplets. The drag coefficient proposed by Wolfe, et al. [7] has the following form:

$$C_D = \frac{4\rho_d D_0^3}{3\rho_g \left(V_g - V_d\right)^2 D_i^2} \frac{dV_d}{dt}$$

where, D_i is the lateral diameter of the distorted droplet.

Wolfe, et al. [7] gave a detailed description of the breakup modes and discussed the effects of droplet relative velocity, droplet properties (e.g., surface tension, viscosity) etc., on the droplet breakup criteria. However, their tests were limited to relatively low Weber numbers, i.e., $O(We) \sim 10^2$. Simpkins and Bales [8] also conducted droplet breakup studies in a shock tube but at much higher Mach numbers of up to 9.0. They were interested in the transition phase between simple distortion (of a droplet) and deformation accompanied by an unstable surface wave, which can grow exponentially with time. Instead of using a Weber number to characterize the

breakup process, the Bond number was preferred (no specific reasons were given), which is written in the following form:

$$Bo = \frac{\rho_d D^2}{\sigma_d}\left(\frac{dV_r}{dt}\right)$$

Their experimental tests were conducted at $Bo > 10^3$ ($\sim We > 10^3$) where instability in the droplet surface waves were known to occur. They concluded with the following findings:

- Droplet response is algebraic (i.e., a phenomenon characterized by either a bag- or hat-like response) when $14 < We < 100$.
- Wave instability is only significant when $Bo >> 10^3$.
- Drag coefficient for a distorting droplet is similar to a rigid sphere for $Re < 10^3$, and $C_D = 2.5$ for $10^3 < Re < 10^5$.

Since these pioneering works, many other researchers [9-15] have also found similar mechanisms of breakup and have developed empirical equations to define the breakup criteria, sizes, fragment velocities, and breakup times. Borisov [9], for example, showed that the critical Weber numbers could vary from 6 to 50, depending on the experimental conditions. He characterized droplet breakup regimes by the droplet sizes produced from the primary breakup process, unlike many others who preferred to use the moment of imminent breakup or complete droplet disintegration. He broadly divided breakup into the following three regimes:

- Regime I to characterize bag type breakup:

$$8 \le We \le 40$$
$$0.2 \le Ra \le 1.6$$

- Regime II to characterize shear type breakup:

$$20 \le We \le 2\text{x}104$$
$$1.0 \le Ra \le 20$$

- Regime III to characterize explosive type breakup:

$$2\text{x}103 \le We \le 2\text{x}105$$
$$20 \le Ra \le 2\text{x}\ 102$$

Regime I corresponds to the division of the initial droplet into two or more secondary droplets with diameters of the same order of magnitude to the initial droplet diameter. Regime II is characterized by the stripping of the droplet surface layer to form new droplets, which are typically considerably smaller than the initial droplet. Regime III involves the explosive breakup of the droplet into droplets, which are significantly smaller than the initial droplet size. Borisov also suggested that, under regime II (shear breakup mode), the time required for the droplet

deformation to reach critical stage (i.e., perforation of the surface by instability waves) for the case of a transient flow (i.e., behind shock wave) could be approximated by:

$$t \approx \frac{D}{V_r}\sqrt{\left(\frac{\rho_d}{\rho_g}\right)}$$

Krzeczkowski [10] used an open-jet horizontal wind tunnel to study breakup where droplets were released at the nozzle exit of the tunnel (i.e., in an open environment). He also studied the effects of fluid viscosity on the breakup modes and times by using methanol, water, butanol, water-glycerin, and glycerin solutions. His experimental data suggested the following four distinct modes of breakup (arranged according to increasing Weber number, see figure B-1 in appendix B):

- bag breakup type, which was characterized by a hollow bag-shaped film and a ring torus.
- bag-jet breakup type, which was similar to the bag form but with an additional stamen appearing in the middle of the bag.
- Transition type, which was characterized by an initial bag type breakup but transformed into the disintegration of the bag film.
- shear (or stripping) type, which was characterized by stripping of the surface layer.

He postulated that all droplet deformation started from the same basic form, which later developed into bag or bag-jet type of breakup, depending on the rate of deformation (i.e., ratio of the longitudinal dimension of the deformed droplet to the initial droplet diameter). Figure B-2 shows an illustration of the different possible transition modes of droplet breakup. Figure B-3 shows the breakup times corresponding to two different modes of breakup for water droplets.

Pilch and Erdman [11] conducted a comprehensive analysis of the experimental data that were obtained by other researchers, and used the data to formulate the five distinct modes of breakup listed below:

- vibrational breakup $We \leq 12$
- bag breakup $12 < We \leq 50$
- bag and stamen breakup $50 < We \leq 100$
- sheet stripping $100 < We \leq 350$
- wave crest stripping $We > 350$
  (followed by catastrophic breakup)

They argued that the breakup of a large accelerating droplet ($We >> 12$) is a multistage process in which fragments (secondary droplets) would undergo further breakup as long as the (fragment) Weber number exceeds the critical Weber number, and upon completion, all the fragments would be smaller than the maximum stable diameter, which is given as follows:

$$d_{\max} = We \frac{\sigma_d}{\rho_g V_r^2}$$

They later improved upon the above equation by taking into account both the fragment size reduction and decreasing relative velocity. The final form of the equation is written as follows:

$$d_{\max} = We \frac{\sigma_d}{\rho_g V_r^2} \left(1 - \frac{V_{frag}}{V_r}\right)^{-2}$$

Pilch and Erdman also suggested that in a multistage droplet breakup, the breakup times consist of the following distinct times:

a. Initiation time (deformation or induction), which is defined as the start of bag formation for bag and bag-stamen breakup; first sign of sheet being drawn downstream for shear breakup; first sign of mist generated on the windward drop surface for wave crest stripping. The initiation time is approximated by

$$T = 1.9(We\text{-}12)^{-0.25}(1+2.2Oh^{1.6})$$

b. Primary breakup time, which is defined as the time when a coherent drop ceases to exist. In the case of the bag breakup, both primary and total breakup times are equivalent, and the intact rim may be viewed as a coherent drop. In shear breakup, a coherent drop should normally exist during the entire breakup process. It is difficult to define the primary breakup time for wave crest stripping due the formation of a mist. The best estimate for primary breakup time is

$$T = 1.25 \quad We > 350$$

c. Total breakup time is defined as the time when the drop and all its fragments no longer undergo further breakup, and the following relationships have been developed for different Weber number ranges:

$$\begin{aligned}
T &= 6.0(We\text{-}12)^{-0.25} && 12 \le We \le 18 \\
T &= 2.45(We\text{-}12)^{0.25} && 18 \le We \le 45 \\
T &= 14.1(We\text{-}12)^{-0.25} && 45 \le We \le 351 \\
T &= 0.766(We\text{-}12)^{0.25} && 351 \le We \le 2670 \\
T &= 5.5 && We \ge 2670
\end{aligned}$$

The total breakup times (defined above) are applicable only to droplets consisting of fluids with low viscosity ($Oh < 0.1$, e.g., water). The nondimensional time, T, is given as follows:

$$T = t \frac{V_r}{D} \sqrt{\left(\frac{\rho_g}{\rho_d}\right)}$$

Wierzba [12] conducted a comprehensive review of the published experimental data and found significant variation in the critical Weber numbers as shown in table 3-1. He suggested that potential sources of error included the use of the droplet radius instead of diameter, incorrect use of the relative droplet-gas velocity, and the incorrect definition of the critical breakup stage, e.g., whether it should be the initiation of droplet deformation or complete breakup stage. He conducted tests to determine the critical Weber numbers (and breakup times) using the horizontal suction wind tunnel shown in figure B-4. Monodispersed water droplets with diameters ranging from 2220 to 3900 μm were released inside the horizontal tunnel. The droplets were subjected to an instantaneous flow (i.e., droplet injected normal to flow). The different stages of droplet breakup were recorded using spark shadowgraph and a high-speed camera. He determined that the critical Weber number (bag breakup) was in the range of 13.7 to 14.07. His results also showed the following breakup modes and times (based on the complete disintegration of a droplet):

- t = 18.21 ms for bag breakup mode
- t = 22.43 ms for vibrational breakup mode
- t = 20.85 ms for the case where an initially vibrational type of breakup was later transformed into bag type of breakup

TABLE 3-1. CRITICAL WEBER NUMBERS (TAKEN FROM WIERZBA [12])

Reference	We_c	Exp. Fac.	Notes
Lenard (1904)	5.8	FF	Calc. for water $-u_\varepsilon = 8\,\text{m/s}$; d_c = 5.5 mm
Merrington and Richardson (1947)	15.4-29.8	FF	Calc. by Hinze (1948)
Lane (1951)	10.8	VWT	Calc from $u_\varepsilon^2 d$ =const. for water
Volynskii (1948)	11-15.8	HWT	Average value 14
Buhman (1954)	2.2-3.6	HWT	For water 2. 6-3.5; (3.9-10.4)
Hinze (1955)	13	HWT	For gas oil
Krzeczkowski (1980)	11-38	HWT	For water 11
Nichiporenko, et al. (1982)	10.9-17.7	HWT	For liquid metal, 17.7 for bag breakup
Wierzba (1985)	14	HWT	For water
Isshiki (1959)	9.26-29	SO	For water 11.1-14.6 = *f (d)*
Haas (1964)	11.2	SO	For mercury
Naida, et al. (1973)	8.4-12.1	SO	Average value for tin 10.9
Yoshida (1985)	10-48	SO	For water 10-31 = *f (d)*
Hanson, et al. (1963)	7.2-47.6	HST	For water 7.2-14.3 = *f (d)*
Simpkins (1971)	13	HST	For water
Gelfand, et al. (1972)	12-16	HST	For liquid nitrogen
Simpkins and Bales (1972)	14	HST	For water
Gelfand, et al. (1973)	10-50	HST	For water 10
Gelfand, et al. (1974)	10	HST	For water and kerosene
Reichman and Temkin (1974)	7	HST	Calc. from $u_\varepsilon^2 d$ = const. for water
Korsunov and Tishin (1971)	15-32	CN	For transformer oil
Lopariev (1975)	14.6-99 6	VS	For low viscosity liquids 14.6-21
Caveny and Gany (1979)	20-30	CN	For Al/Al_2O_3 agglomerates
Borisov, et al. (1986)	40-60	HST	For water and kerosene

FF: free fall experiments HWT: horizontal wind tunnel SO: suction orifices, VS: venturi scrubber
VWT: vertical wind tunnel HST: horizontal shock tube CN: convergent nozzle

The vibrational breakup mode that was reported by Wierzba [12] was also the main focus of the experimental investigation conducted by Hirahara and Kawahashi [13]. They were particularly interested in the mechanism of droplet breakup below Weber number 13.0. The tests were conducted in a shock tube with droplet diameters between 2200 and 3900 μm. Both water and silicon oil was used to study the effects of fluid viscosity on droplet breakup. The results obtained from high-speed images showed that droplet breakup occurred at *We* ~10, which was below the values found by other researchers, e.g., Krzeczkowski [10], Pilch [11] and Wierzba [12]. Hirahara and Kawahashi also found that tests conducted at *We*~7.1 exhibited no breakup although the droplet shape was distorted. Contrary to Pilch, et al. findings [11], they concluded that the droplet deformation time was independent of the Weber number, although they confirmed Wolfe and Andersen's finding that deformation of droplet depended on both pressure distribution and shearing stress on the droplet.

The experimental investigations that have been reviewed thus far were conducted using shock tubes and horizontal tunnels where droplets were subjected to an instantaneous air flow. Vertical wind tunnels have also been used to study droplet breakup. Kennedy and Roberts [14], for example, used a vertical wind tunnel (figure B-5, in appendix B) to study breakup where droplets were subjected to an accelerating flow. These investigators were interested in simulating rain droplet ingestion into gas turbine engines, therefore, maintaining relative droplet-gas velocity was deemed the most important parameter of the experimental test. Water droplets with diameters between 500 and 3000 μm were released under gravity at the tunnel inlet and were accelerated by converging walls toward the throat (of the tunnel) where breakup occurred. The throat velocities of the tunnel were varied from 20 to 125 m/s (70 to 408 ft/s). They also used the Rabin number to characterize droplet breakup instead of the Weber number. Their experimental data showed that the following Rabin number threshold values could be used to define bag and shear breakup (see figure B-6):

- $Ra = 0.4$ for hat (bag) breakup mode
- $Ra = 0.79$ for shear (stripping) breakup mode

Although the experimental data of Kennedy, et al. was related to the relative velocity between the droplet and gas, the effects of a time-dependent (varying) relative velocity on the critical Weber number and breakup time was not investigated. Suzuki and Mitachi [15] studied these effects by releasing droplets into the unsteady droplet-gas velocity flow of an orifice plate. They reported results for the following test cases:

a. Relative droplet-gas velocity rose to constant (settling) value within a finite time (figure B-7).

b. Relative droplet-gas velocity increased linearly with time (figure B-8).

In case (a), they found that the breakup mechanism (e.g., bag, shear, explosive, etc.) depended on the rise time and settling value of the relative droplet-gas velocity but the critical Weber number (e.g., *We* ~13) was relatively independent of the rise time. However, the breakup time generally decreased with increasing *We* number (figure B-9). In case (b), the critical Weber number (at the moment of breakup) was greater than the critical value for a constant velocity flow field, and it

increased with increasing rate of relative droplet-gas velocity (figure B-10). This is higher than the known critical Weber number range of 13 to 14, which may also offer an explanation to the vast range of critical Weber number values shown in table 3-1. Suzuki and Mitachi [15] concluded that critical Weber numbers available from published literature were not sufficiently accurate in cases where relative droplet-gas velocity varied with time.

A review of the published literature was presented, and it is believed that the experimental tests conducted by Kennedy and Roberts [14] and Suzuki and Mitachi [15] bear some similarities to the conditions experienced by droplets near an airfoil. For example, when an aircraft flies into an icing cloud, droplets located near the stagnation regions of the aircraft, e.g., wing, tail, etc., will experience an increasing pressure force that is similar to the test conditions in the vertical tunnel (Kennedy and Roberts's test facility [14]) and orifice plate (Suzuki and Mitachi's test facility [15]). In summary, the literature review conducted indicates the following:

- Droplet breakup can be characterized with nondimensional Weber, Rabin, and Bond numbers. The most commonly used test facilities for conducting droplet breakup experiments were shock tubes and horizontal tunnels.

- Critical values (of *We*, *Ra*, and *Bo*) can vary depending on the experimental test facility (see table 3-1) and the methodology employed to define droplet breakup. Critical Weber number can be greater when relative droplet-gas velocity varies with time*.

- Droplet can undergo a multistage breakup as long as the fragment sizes continue to exceed critical values. The breakup (or fragment) sizes can be defined with empirical correlations, e.g., Wolfe, et al. and Pilch, et al.

- Droplet breakup time consists of the initiation (deformation) and primary breakup times. The total breakup time is defined as the time required for complete disintegration of a droplet. The breakup time can be approximated with empirical correlations, e.g., Wolfe, et al. and Pilch, et al.

* Based on the publication of Suzuki, et al. [15].

4. SELECTION OF DROPLET BREAKUP MODEL.

This section presents a computational study conducted to assess the performance of droplet breakup models that are available in two commercial computational fluid dynamic (CFD) codes used by the icing group at Wichita State University: STAR-CD (CD Adapco Group) and FLUENT (Aavid Thermal Technologies Inc.). The purpose of the study was to select one of the models for conducting droplet breakup simulations near an airfoil. The selection process was based on the ease of application and time required for familiarization with the selected model. A brief description of the breakup models in the two CFD software packages used is provided below. Further details of these models can be found in appendix C.

4.1 SOFTWARE SELECTION—FLUENT VS STAR-CD.

The STAR-CD software is a relatively new CFD computer code compared to the well-established FLUENT code. Both codes solve the Navier-Stokes equations using the finite volume technique. The numerical algorithms and techniques employed by both codes are almost identical. However, there are major differences in the choice of droplet breakup models available in these codes. To assess the performance of the STAR-CD software, an academic license for Microsoft Windows 2000® operating system, version 3.15A, was obtained from the vendor. Wichita State University already has access to FLUENT version 6.18, for Microsoft Windows 2000.

4.1.1 STAR-CD Version 3.15A (Windows 2000).

This CFD software offers three different empirical droplet breakup models (details are given in appendix C, section C.1):

- Pilch and Erdman [11]
- Reitz and Diwaker [16]
- Hsiang and Faeth [17]

The Pilch and Erdman model provides five distinct breakup modes (section 3) that vary with Weber numbers. Each breakup mode also includes an equation for calculating the breakup time. The software computes the conditions for droplet breakup during each time step until the breakup process has been completed and a stable droplet fragment size has been reached. The maximum stable droplet size is given by the following equation:

$$d_{\max} = We \frac{\sigma_d}{\rho_g V_r^2} \left(1 - \frac{V_{frag}}{V_r} \right)^{-2} \tag{4-1}$$

The Reitz and Diwaker model [16] assumes that droplet breakup can occur either in the bag or shear (stripping) mode. For the bag mode, breakup occurs when the droplet Weber number exceeds a critical value ($We \geq 12$), and for the shear mode, when the Rabin [18] number is greater than 1.0). The stable droplet diameter, D_s, is that which satisfies the equality in the following equation:

$$\frac{\rho g \cdot \left| v_g - d_d \right| \cdot D_s}{\sigma_d} = 12 \tag{4-2}$$

Hsiang and Faeth's model [17] is applicable for droplet breakup in conditions similar to those found in diesel engines, hence, valid for *We* < 1000. Breakup occurs when the Weber number exceeds a critical value (i.e., *We* > 12). The stable droplet size is given by the following equation:

$$D_{\max} = 6.2 \cdot D \cdot \left(\frac{\rho d}{\rho g} \right)^{\frac{1}{4}} \cdot \sqrt{\frac{\mu_d}{D \cdot \rho_d \cdot \left| v_g - v_d \right|}} \tag{4-3}$$

Equations for calculating the breakup time are provided by all three models. The drag coefficient (in all three models) is based on a perfect sphere.

An effort was conducted to evaluate the functionality of the STAR-CD software and to determine how to use the breakup models. The application of the breakup model required a flow-field solution for droplet trajectory analysis. The trajectory analysis is followed by the computation of droplet breakup. After having spent the allocated time (~2 months) on this task, it was concluded that this version (3.15A) of the STAR-CD was not well developed for Windows 2000, a fact that is recognized by the software supplier. In general, the functional performance of the software was unpredictable and prone to computer crashes. Although progress was made in the computation of the flow field and droplet trajectory (with no breakup), little progress was made with the breakup models. Due to limited resources, it was decided to abandon this effort and to proceed with the evaluation of the breakup model in the FLUENT software.

4.1.2 FLUENT Version 6.18.

This CFD software provides two droplet breakup models (appendix C, section C.2):

- O'Rouke and Amsden's TAB model [19]
- Reitz's Wave Breakup model [20]

The TAB model assumes that droplet oscillatory motion is analogous to that of a damped spring-mass system undergoing a forced oscillatory motion. The mathematical equation that describes this kind of motion can be written as follows:

$$F - kx - d\frac{dx}{dt} = m\frac{d^2x}{dt^2} \tag{4-4}$$

where *x* is the displacement of a point located at the equator of an initially perfect sphere, as illustrated in figure 4-1.

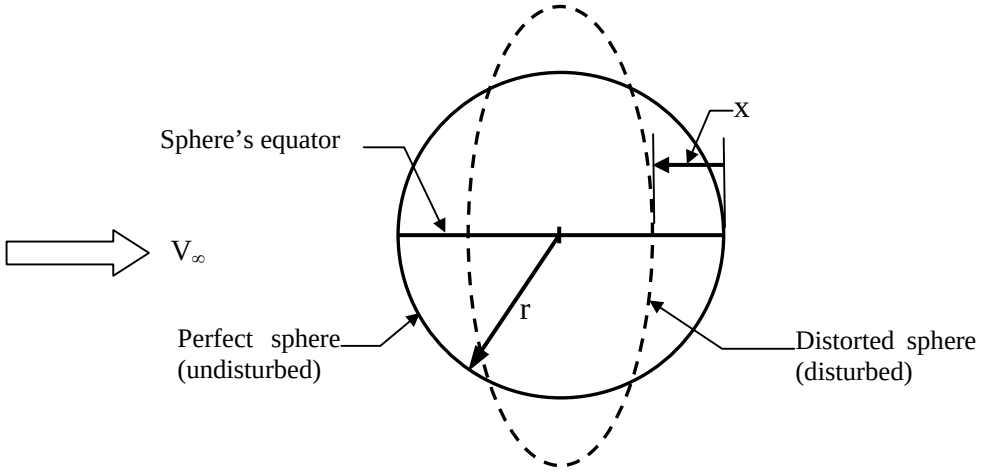

FIGURE 4-1. DISTORTION OF A DROPLET SUBJECTED TO PRESSURE FORCES

The external force (F) in equation (4-4) is the dynamic pressure force of the flow field exerted on the droplet, the restoring force (kx) is due to the droplet surface tension, and the damping force ($d\frac{dx}{dt}$) is due to the droplet viscosity. Droplet breakup is assumed to occur when the displacement (x) is equal to the half-radius of an undisturbed droplet:

$$x = 0.5\, r \tag{4-5}$$

Two forms of the drag coefficient are provided with the TAB model, one is based on that for a perfect sphere and the other is based on a distorted droplet to account for the increased in drag when the droplet is flattened into a disk. Although the FLUENT software computes the breakup size and time, only the droplet breakup size is available to the user. The wave model (Reitz and Bracco [21]) was developed from the analysis of the jet stability in the breakup of a cylinder jet of water. The model assumes that the breakup time and size are related to the fastest growing Kelvin-Hemholtz instability and is applicable only for very high-speed injections.

After an initial familiarization period, it was found that the TAB model can be applied to many different kinds of flow environments, e.g., isolated airfoil, tunnel, etc. The gaseous phase (or air flow) was computed prior to the droplet trajectory and breakup computations. FLUENT employs a time-marching technique to compute a droplet's spatial location, velocity, distortion (with TAB), and other scalar properties (temperature, density, etc.) in a given flow field.

In the final assessment, the choice of the CFD software was limited only to FLUENT due to the problems associated with the STAR-CD Windows 2000, version 3.15A. In view of the limited time and resources available, the FLUENT software was selected for conducting the droplet breakup studies presented in this report.

4.2 FEATURES AND LIMITATIONS OF THE TAB MODEL.

The numerical formulation of the TAB model can be found in appendix C, section C.2. Listed below are the summarized features of the model.

- The model does not define droplet breakup with a unique critical Weber number, such as Weber of 13. The breakup process depends on the history of the relative droplet-air velocity and droplet lateral diameter ($x = 0.5\ r$ in figure 4-1).

- The droplet viscosity is also included in the differential equation unlike empirical models such as Pilch's correlations in which the viscosity is ignored.

- The model is applicable for droplet Weber numbers less than 100.

- The model predicts the state of oscillation and distortion only. It can only simulate one oscillation mode, which corresponds to the lowest order spherical zonal harmonic. In reality, there may be many more oscillatory modes, but there are no published reports that indicate the number of possible modes.

- The drag coefficient of the droplet can be corrected for droplet distortion, which generally occurs with larger rather than smaller droplets.

- Predicted droplet breakup sizes are known to be consistent with experimental measurements.

Limited comparison of the droplet sizes predicted with the TAB and Reitz models has been made with the experimental data obtained by Hiroyasu and Kadota [22] (based on one datapoint). The results showed that the predicted droplet sizes from both models showed relatively good agreement with the available experimental data. In general, the breakup sizes obtained with the Reitz and Diwaker's model were in slightly better agreement with the experiment than those predicted by the TAB model. However, O'Rouke [19] (author of the TAB model) argued that reducing droplet breakup sizes (by increasing the K value in equation C-14 in appendix C) might improve the accuracy of the predicted values.

5. VALIDATION OF THE TAB MODEL.

In section 4.2, the features and limitations of the TAB model were presented. An attempt was made prior to the start of the droplet breakup parametric study to explore and validate some of the key assumptions made in the TAB model and to compare the critical breakup conditions, such as the Weber and Rabin numbers and breakup times, with the published experimental data. It must noted that the TAB model determines the moment of critical breakup from the degree of droplet distortion and relative droplet-air velocity (equation C-2, appendix C), and not from the critical Weber (e.g., $We \sim 13.0$) or Rabin numbers (e.g., $Ra \sim 0.4$).

Although a majority of the reported droplet breakup studies were conducted in shock flow test facilities (see section 3), it was not possible to use the experimental data to validate the TAB model since the droplets were subjected to the aerodynamic forces that far exceeded those found near airfoils, whereas the flow conditions in the current study are expected to be subsonic. In addition, there is also a lack of published technical details on the test facilities and test conditions, therefore, it is not possible to perform any kind of validations. However, adequate details on the test facilities and conditions were reported by Wierzba [12] (droplet breakup tests conducted in a vertical tunnel facility) and Kennedy, et al. [14] (droplet breakup tests conducted a horizontal tunnel); therefore, they were selected for validating the TAB model. In the work of Wierzba [12], details regarding the initial droplet sizes, breakup modes, breakup times, high-speed images, etc., are readily available. In addition, in the horizontal tunnel tests, droplets were subjected to a shear flow field, which is considered similar to that experienced by droplets traveling near an airfoil at high angle of attack (AOA) or a three-element airfoil where the slat and flap were deployed. The vertical tunnel test facility (as reported by Kennedy, et al. [14]) was selected since the droplet breakup conditions in an accelerating flow are also similar to those experienced by droplets traveling towards the stagnation region of an airfoil. Although droplets in the case of an airfoil would be subjected to a decelerating flow field, droplet breakup behavior depends mainly on the relative velocities between the droplet and free-stream airflow, not on whether the flow is accelerating or decelerating.

5.1 HORIZONTAL WIND TUNNEL (WIERZBA [12]).

Wierzba conducted an experiment to determine the critical Weber number for droplet breakup and the droplet breakup time using a horizontal suction wind tunnel. Figure B-4 in appendix B shows the test facility and instrumentation that were used to study droplet breakup. The test section consisted of an 8- by 8-cm-square section pipe. Air entered the tunnel from an enclosed large chamber that was supplied from a compressor (located upstream of the chamber). A flare inlet bell-mouth was used to maintain uniform velocity profile at the test section. A monodispersed droplet generator was mounted on top of the square section pipe. The author did not define the droplet release location or droplet injection velocity. Droplet breakup was recorded using a spark shadowgraph and a high-speed camera.

A two-dimensional (2D) computational grid of the test facility is shown in figure 5-1. This grid was constructed to investigate droplet breakup with the TAB model. Local clustering of the mesh points was applied near the pipe wall to simulate the near-wall boundary layer flow. The flow field was computed with the FLUENT code using the following conditions:

- Velocity inlet and pressure outlet boundaries
- RNG k-ε turbulence model
- Compressible ideal gas
- Sutherland viscosity equation

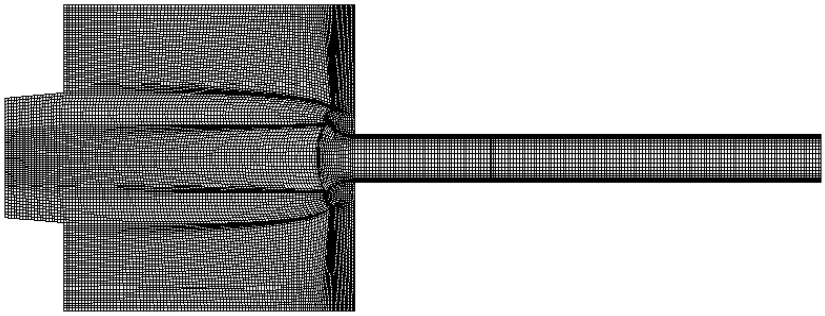

FIGURE 5-1. TWO-DIMENSIONAL MODEL OF A HORIZONTAL TUNNEL

Figures 5-2 and 5-3 show contours of the predicted velocity and pressure distributions in the tunnel respectively. Monodispersed droplets were released at about 40 cm downstream of the flare-inlet (~5 pipe diameters). Figure 5-4 shows the velocity profile plotted at the droplet release location. (The author of the experimental study did not present any measurements of the tunnel velocity profile at the droplet release plane.) The tracking of the droplet trajectory (and breakup) was carried out using a time-marching technique in the FLUENT software. In simple terms, a single droplet was released into the gas flow at a fixed location in the flow field and at regular time intervals to simulate a continuous stream of droplets. This was done by introducing a new droplet at the desired location during each time step of the droplet trajectory integration process. At each time-step, distortion of the droplets and the associated increase in drag was computed using the TAB model. The low droplet concentration used in the simulation avoided the need to include the effects of the droplets on the flow field. Water droplets with diameters of 2220, 2600, and 3900 μm were released under gravity at the predefined location. Figures 5-5 to 5-7 show the droplet sizes as they traversed across the boundary layer of the gas flow.

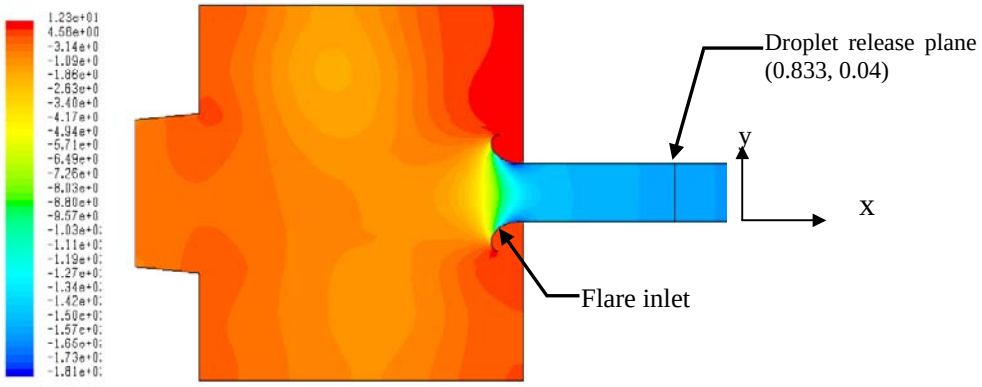

FIGURE 5-2. PREDICTED PRESSURE CONTOURS IN HORIZONTAL TUNNEL

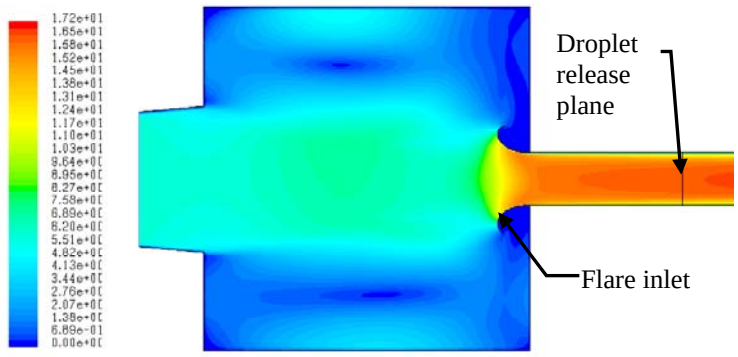

FIGURE 5-3. PREDICTED VELOCITY CONTOURS IN HORIZONTAL TUNNEL

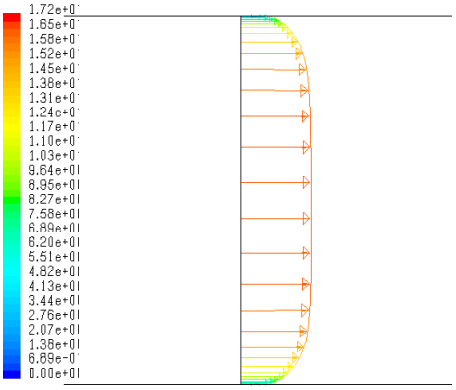

FIGURE 5-4. VELOCITY PROFILE PLOTTED AT THE DROPLET RELEASE PLANE

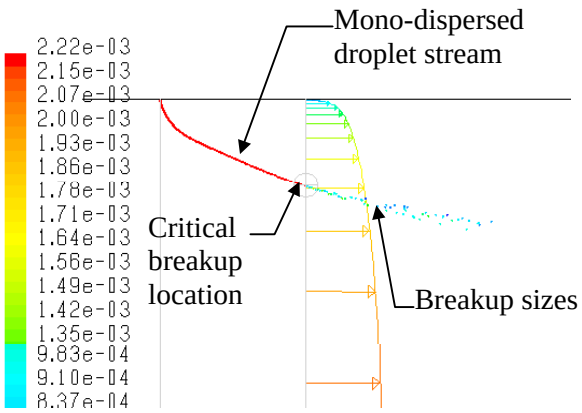

FIGURE 5-5. PREDICTED DROPLET TRAJECTORY AND SIZES, D = 2220 μm

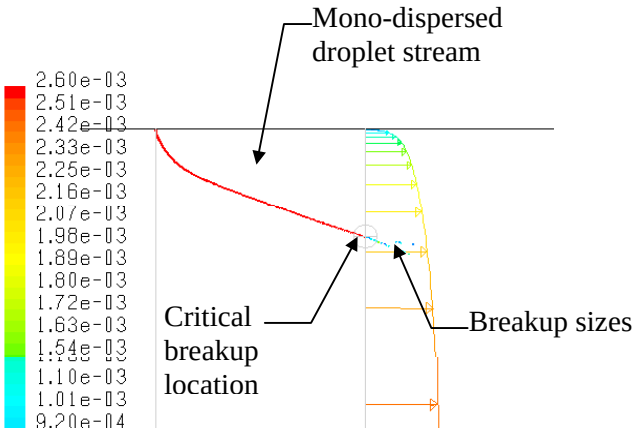

FIGURE 5-6. PREDICTED DROPLET TRAJECTORY AND SIZES, D = 2600 μm

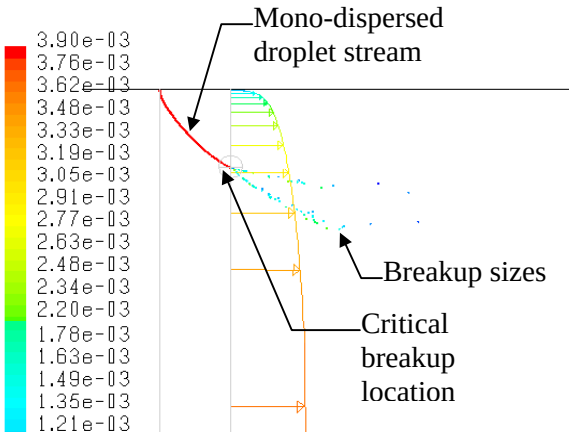

FIGURE 5-7. PREDICTED DROPLET TRAJECTORY AND SIZES, D = 3900 μm

The trajectory plots in figures 5-5 to 5-7 show a small dispersal of fragmented droplets, which is due to the imposition of a normal component velocity to the fragmented droplets by the TAB model. The critical Weber number (for each droplet size) was computed with the droplet and air velocities taken at the moment just prior to breakup. An estimate of the droplet breakup times was also computed using the correlations from Pilch and Erdman [11] (section 3). Table 5-1 shows the relative droplet-gas velocities, ratio of breakup sizes to the initial droplet diameters, breakup times and critical Weber numbers.

TABLE 5-1. HORIZONTAL TUNNEL (PREDICTED AND EXPERIMENTAL VALUES)

Initial droplet y-velocity = -0.1 m/s Initial *x* distance = 0.833 m, Initial *y* distance = 0.04 m			
Droplet initial diameter (μm)	2220	2600	3900
Axial breakup distance *x* (m)	0.843	0.849	0.845
Vertical breakup distance *y* (m)	0.031	0.025	0.028
Droplet breakup velocity V_d (m/s)	0.914	1.130	1.170
Air flow velocity V_g (m/s)	17.00	17.50	17.00
Average droplet breakup diameter (% / μm) Initial droplet diameter	3.8/85	3.8/100	3.9/150
We (predicted)	9.4	11.4	16.0
We (measured)	*We*~13.7 to 14.07 (Wierzba [12])		
Predicted breakup time (Pilch and Erdman's) (ms)	28	32	30
Measured breakup times (ms)	18.21 to 22.43 (Wierzba [12])		

5.2 VERTICAL WIND TUNNEL (KENNEDY AND ROBERTS [14]).

In previous studies, researchers have often used shock tubes and horizontal tunnels to investigate droplet breakup through the viscous interaction with an instantaneous flow. However, Kennedy, et al. [14] used a vertical tunnel facility to study droplet breakup, as shown in figure B-5 in appendix B. The converging walls of the contraction section of the tunnel accelerated the air at the throat to velocities of up to 125 m/s (408 ft/s). The experimental results obtained are shown in figure B-6. To validate the TAB model with these experimental data, a 2D model of the test facility was created, as shown in figure 5-8. The dimensions of the test facility are shown in figure 5-9. The tunnel flow field was computed with the FLUENT CFD software using the following conditions:

- Velocity inlet and pressure outlet boundaries
- RNG k-ε turbulence model
- Compressible ideal gas
- Sutherland viscosity equation

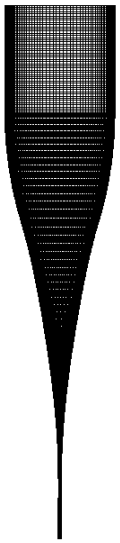

FIGURE 5-8. TWO-DIMENSIONAL MODEL OF A VERTICAL TUNNEL

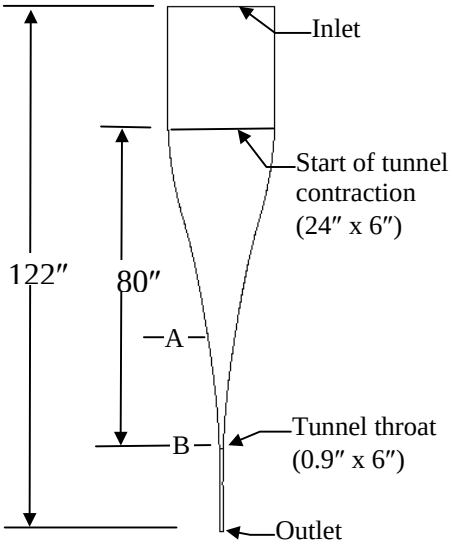

FIGURE 5-9. DIMENSIONS OF THE VERTICAL TUNNEL

The shape of the tunnel contraction was computed by trial and error since it could not be found in the published report. The simulated droplet velocity in the center of the contraction was compared with published data reported for droplet diameters of 500, 1000, and 1600 μm. Appropriate changes to the shape of the contraction walls were made until agreement in the simulated droplet velocity values were found, as shown in figure 5-10a to 5-10c.

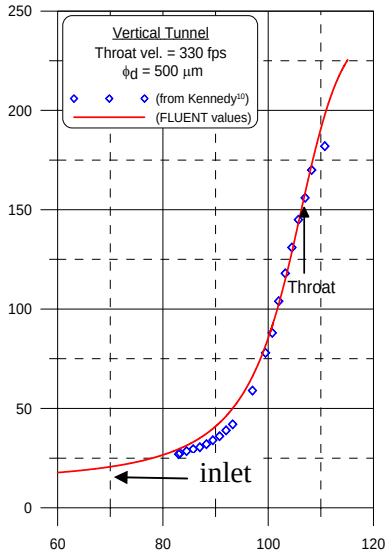

FIGURE 5-10a. SIMULATED DROPLET VELOCITY, D = 500 μm, THROAT VELOCITY = 330 ft/s

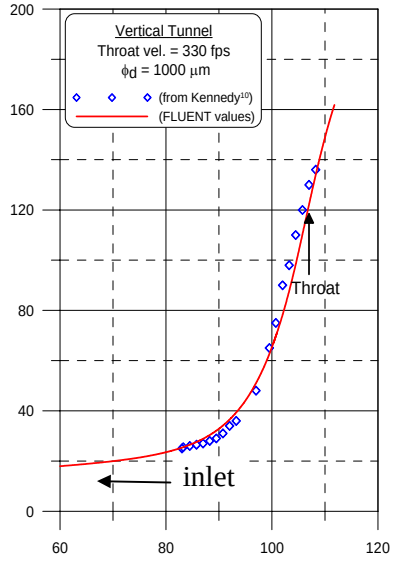

FIGURE 5-10b. SIMULATED DROPLET VELOCITY, D = 1000 μm, THROAT VELOCITY = 330 ft/s

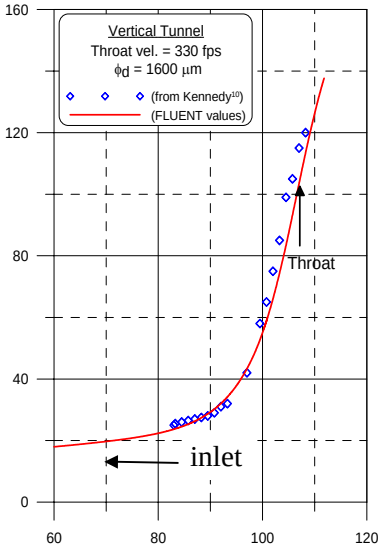

FIGURE 5-10c. SIMULATED DROPLET VELOCITY, D = 1600 μm, THROAT VELOCITY = 330 ft/s

Figure 5-11 shows pressure contours for the tunnel flow field, and figure 5-12 shows the velocity profile plotted at the throat of the convergent section. Droplet breakup was simulated at several tunnel velocities with droplet diameters between 500 and 1991 μm. Typical plots of droplet sizes are provided in figures 5-13 and 5-14, which show the breakup of 500 and 948 μm droplets at a tunnel velocity of 330 ft/s respectively. Table 5-2 gives the critical Rabin numbers, simulation conditions, and other relevant parameters computed with the TAB model. The critical Rabin values were based on the moment just before breakup began, as shown in figures 5-13 and 5-14. Figure 5-15 (plotted from table 5-2) shows the predicted and measured critical values of the Rabin numbers for several droplet sizes and throat velocities.

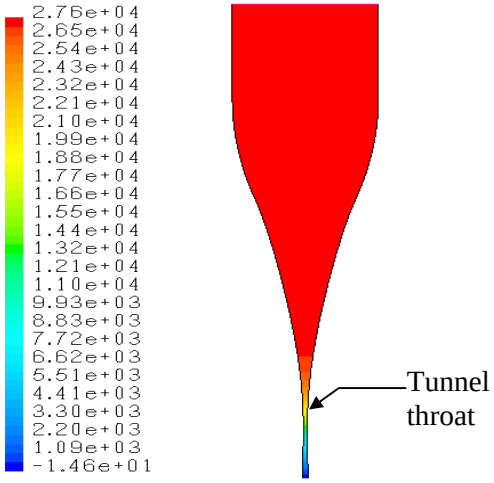

FIGURE 5-11. PRESSURE CONTOURS, THROAT VELOCITY = 330 ft/s

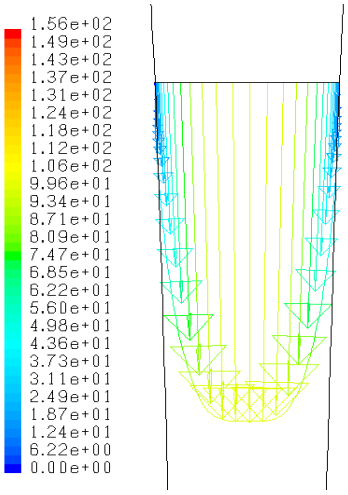

FIGURE 5-12. VELOCITY PROFILE PLOTTED AT TUNNEL THROAT

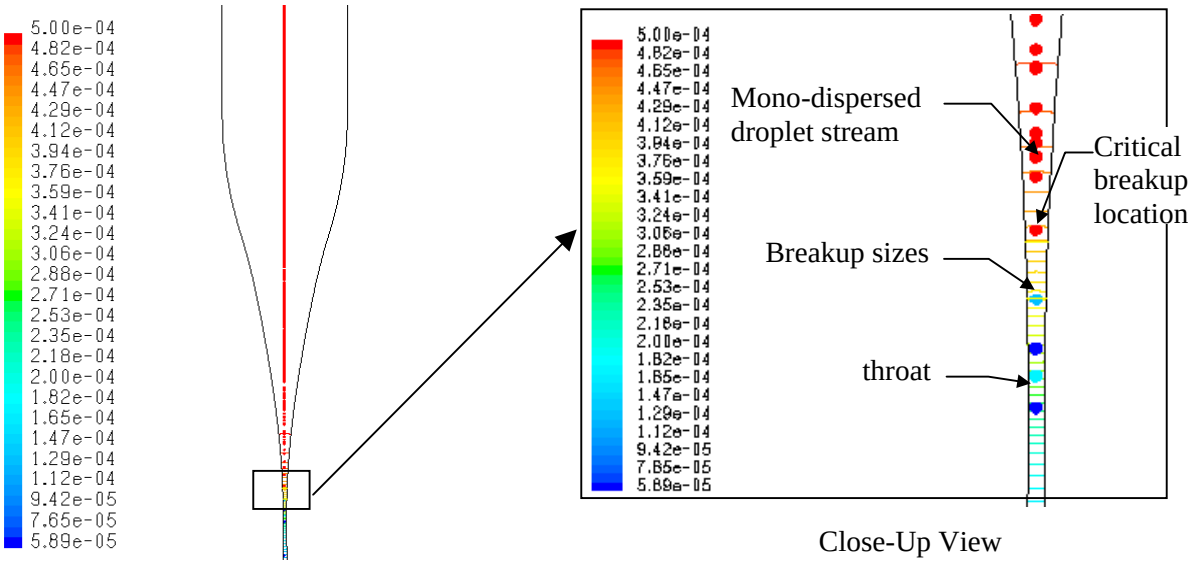

FIGURE 5-13. SIMULATED DROPLET BREAKUP, D = 500 μm, THROAT VELOCITY = 330 ft/s

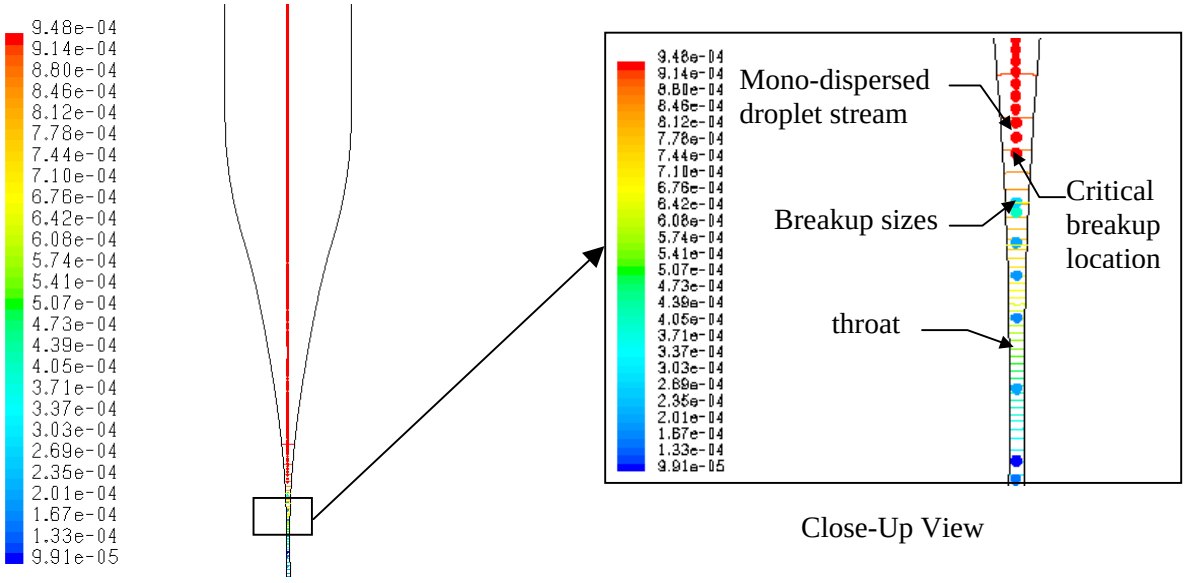

FIGURE 5-14. SIMULATED DROPLET BREAKUP, D = 948 μm,
THROAT VELOCITY = 330 ft/s

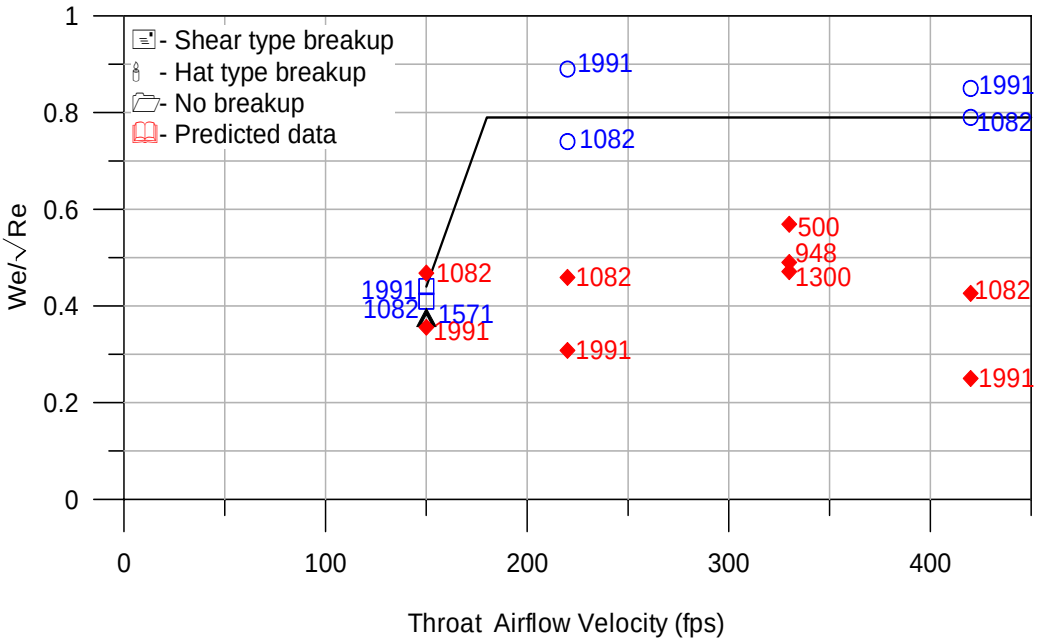

FIGURE 5-15. MEASURED AND PREDICTED BREAKUP CRITERION

TABLE 5-2. VERTICAL TUNNEL (PREDICTED AND EXPERIMENTAL VALUES)

Throat velocity (ft/s)	150		220		330			420	
Droplet release velocity (ft/s)	0.3		0.3		0.3			0.3	
Droplet initial diameter (μm)	1082	1991	1082	1991	500	948	1300	1082	1991
Breakup distance above throat, Δy (m)	0.0585	0.0813	0.0353	0.180	0.01760	0.1232	0.1659	0.24505	0.4327
Droplet breakup velocity V_d (m/s)	19.9	10.2	18.7	9.66	39.4	21.6	17	18.7	10.3
Air flow velocity V_g (m/s)	56.7	35.2	55	32.35	93.5	61.25	51.75	53.25	30.06
We	23.97	20.35	23.32	16.77	23.94	24.38	25.68	21.13	12.72
Re	2618	3273	2583	2971	1779	2472	2971	2458	2587
$Ra=\frac{We}{\sqrt{Re}}$ (predicted)	0.468	0.356	0.459	0.308	0.568	0.49	0.471	0.426	0.25
$Ra=\frac{We}{\sqrt{Re}}$ (measured)	0.4	0.45	0.74	0.89	0.79	0.79	0.79	0.79	0.85

5.3 RESULTS AND DISCUSSION.

For the studies conducted in the horizontal tunnel, the simulations in figures 5-5 to 5-7 show that the droplets were subjected to an instantaneous air flow from the moment of release, and breakup occurred near the outer edge of the boundary layer where uniform velocity was found. The fragmented droplets were simulated as a number of smaller droplets with (average) diameters of 85, 100, and 150 μm for the initial droplet diameters of 2220, 2600, and 3900 μm respectively. This characteristic small number of fragmented droplets seem to concur with the bag (or hat) type of breakup as observed by Wierzba [12]. (The experimental breakup sizes were not reported, therefore, no comparison could be made.) Table 5-1 shows the comparison between measured and predicted critical Weber numbers and droplet breakup times. The measured Weber numbers were between 13.7 and 14.07, whereas the predicted (TAB) values were 9.4, 11.4, and 16.0 for initial droplet diameters of 2220, 2600, and 3900 μm respectively. The comparative results seem to show relatively good agreement between the measured and predicted critical Weber numbers. It must be noted that the condition of complete droplet breakup was used to determine the critical Weber number in the experiments. However, this condition cannot be used in the simulations since the model lacks the fidelity necessary for simulating this level of detail. Therefore, Weber numbers were calculated at the location of imminent droplet breakup. The comparison between predicted and measured droplet breakup times demonstrates relatively good agreement. The measured droplet breakup times were between 18.21 and 22.43 ms, whereas the predicted times were between 28 and 30 ms.

The simulations conducted with the vertical tunnel (Kennedy, et al. [14]) showed that droplet breakup tends to occur in the contraction section of the tunnel, just upstream of the throat. Table 5-2 gives the different heights above the tunnel throat where droplet breakup occurred for a range of simulated conditions. In general, the simulated results presented indicate that large

droplets breakup earlier than smaller droplets as shown in figures 5-13 and 5-14 for large (D = 948 μm) and small droplets (D = 500 μm) respectively. The breakup process created only two or three smaller droplets, a phenomenon characterized by the vibrational breakup mode. Kennedy, et al. [14] did not publish any information on the number of droplet fragments or the methodology used to define breakup. They only reported the following experimental measurements (figure 5-15):

- Ra = 0.4 for hat (bag) breakup mode
- Ra = 0.79 for shear (stripping) breakup mode)

Measured and predicted critical Rabin numbers are provided in table 5-2. Figure 5-15 shows the Rabin numbers plotted as a function of the air velocity at the tunnel throat. For a throat velocity of 150 ft/s, the predicted Rabin numbers ($0.4 < Ra < 0.5$) were in good agreement with the experimental data ($0.36 < Ra < 0.47$). In addition, the bag (or hat) breakup mode predicted by the code was also observed in the experimental tests at these Rabin values. As the tunnel air velocity was increased from 150 ft/s to 420 ft/s, the computed Rabin numbers ranged from 0.3 to 0.6, whereas the experimental values ranged from 0.7 to 0.9. There are several reasons for the lower Rabin numbers predicted by the code:

- The TAB model cannot simulate shear type of breakup, which was found in the experimental tests at throat velocities greater than 150 ft/s.

- The condition of imminent droplet breakup used to compute the critical Rabin number in the simulations might be incorrect. It is known that improper selection of conditions for droplet breakup can lead to large errors in the calculation of the critical breakup values.

The predicted critical Weber numbers were between 12.72 and 25.68 (Kennedy, et al. [14] did not provide Weber numbers). The lower range of the critical Weber numbers seems to show good agreement with critical breakup values found in published literatures (section 3). The higher predicted Weber number seems to concur with Suzuki, et al. [15] finding that critical Weber number in a linearly increasing flow field (as in the vertical tunnel) can be greater than that obtained in a constant velocity flow field.

In summary, the comparison between predicted and experimental data from the two different test facilities shows that the TAB model is capable of simulating the droplet breakup process with acceptable level of accuracy. The Weber numbers computed from critical droplet breakup conditions predicted with the TAB model in the horizontal tunnel were between 9.4 and 16.0, whereas the experimental measurements were between 13.7 and 14.07. Although the TAB model does not employ a critical Weber number to determine breakup criteria, generally good agreement was found in the Weber numbers obtained from the TAB model and the experimental data. In addition, the experimental studies used to validate the TAB model were conducted at conditions where vibrational and bag breakup modes were observed. Since the size distribution of the fragmented droplets was not reported in the experimental studies, no comparison could be made to ascertain the sizes of the predicted droplet fragments obtained with the TAB model. The analysis from the vertical tunnel also seems to support the results of the simulations performed. When the breakup modes and critical Rabin numbers from the analysis and experiment were compared for a tunnel velocity of 150 ft/s, good agreement was found. For the

bag breakup mode reported in the experiment, the measured Rabin number was in the range of 0.36 to 0.47, while the predicted Rabin number ranged from 0.4 to 0.5. However, at tunnel velocities greater than 150 ft/s, shear breakup modes were obtained with Rabin numbers between 0.7 and 0.9, while the predicted Rabin values were between 0.3 and 0.6, hence, under-predicted. It is thought that the TAB model may not be suitable for modeling droplet breakup (in the current study) where shear breakup modes are more likely to occur because it is limited to vibrational and bag modes only. The range of critical breakup Weber and Rabin numbers found in the published literature (section 3.0) for these two breakup modes are listed below.

- Borisov [9]: $8 \leq We \leq 40$, $0.2 \leq Ra \leq 1.6$ for bag breakup mode

- Pilch and Erdman [11]: $We \leq 12$ for vibrational breakup mode
  $12 < We \leq 50$ for bag breakup mode

- Wierzba [12]: $13.7 < We < 14.07$ for bag breakup

- Kennedy, et al. [14]: $Ra = 0.4$ for hat (or bag) breakup mode

In general, the predicted Weber and Rabin numbers ($9.4 < We < 16.0$, $0.4 < Ra < 0.5$) for vibrational and bag breakup modes were within the range of the reported values shown above. It is also believed that similar critical breakup values would have been found with the empirical breakup model in the STAR-CD software, which is the Pilch and Erdman [11] breakup model discussed in appendix C, section C.1. The effects of the near-wall shear flow on the droplets traversing the boundary layer in the horizontal tunnel test facility are similar to those experienced by droplets traversing the shear boundary layer near the airfoil surface. The effects of the decelerating flow near the stagnation region of an airfoil on droplet breakup are similar to those experienced by droplets being subjected to the accelerating flow of the vertical tunnel. Therefore, the selected test cases were deemed suitable for validating the TAB model and the findings show that this model is suitable for simulating droplet breakup in airfoil flow fields as long as the mode of breakup is of the vibrational or bag type.

6. DROPLET BREAKUP ANALYSIS.

It was shown earlier that the TAB model is capable of simulating droplet breakup with acceptable accuracy and that the predicted breakup modes are limited to vibrational and bag types only. However, it is not known what type of breakup (besides vibrational and bag) could be expected near an airfoil due to the lack of experimental data. In addition, it is also not known whether the simulation is sensitive to computational grid resolution or to the initial droplet release location with respect to the airfoil. To assess the effect of these unknowns on the computed results, studies were performed initially with large water droplets and a NACA0012 airfoil with a chord length (20 ft) representative of large transport aircraft. These parameters were selected to enhance the breakup process since the resulting aerodynamic forces (near the airfoil) and the corresponding Weber numbers would be sufficiently large to induce droplet breakup. The findings from these initial assessments (e.g., optimum grid resolution and droplet release location) were then applied to the simulation of droplet breakup for two NACA0012 airfoils with chord lengths of 3 and 20 ft, and a three-element airfoil with chord length of 20 ft. Monodispersed droplets with diameters of 100, 500, and 1000 μm were released upstream of the airfoil. These droplet sizes are representative of the approximate maximum droplet size in 14 CFR Part 25, Appendix C icing clouds, threshold size between freezing drizzle and rain, and the maximum droplet size applicable to the TAB model (from section 5) respectively. The details of the analyses are in appendix D.

6.1 EFFECTS OF GRID RESOLUTION AND DROPLET RELEASE LOCATION ON DROPLET BREAKUP.

In section 5, the TAB model was applied to droplet breakup simulations in horizontal and vertical tunnel flow fields where the geometry of the test facilities and run conditions were quite well defined, e.g., height and width of tunnel, tunnel velocity, and droplet size were known a priori. In the application of the TAB model to droplets in an isolated airfoil flow field, the physical domain is much greater, and it is not known whether the resolution of the computational mesh or the droplet release location (with respect to the airfoil) would affect the accuracy of the simulation. To assess this, a limited study was performed with a 2D NACA0012 airfoil (figure 6-1a) with a chord length of 20 ft. It is thought that using a large airfoil would promote droplet breakup due to the presence of greater pressure gradients and, therefore, forces in the proximity of the airfoil. Droplets with a diameter of 1000 μm (only) were used to further enhance the possibility of droplet breakup due to higher Weber numbers associated with large droplets.

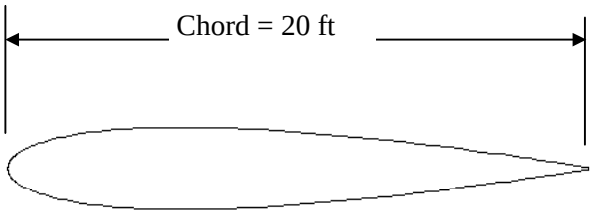

FIGURE 6-1a. NACA0012 AIRFOIL

To assess the effect of grid resolution on droplet breakup, three computational meshes with 136,000, 200,000, and 300,000 grid points were generated around the NACA0012 airfoil as shown in figure 6-1b. The flow field in the computational mesh was computed with the FLUENT CFD software. Figure 6-1c shows pressure distributions obtained with each computational mesh. A group of monodispersed (single-sized) droplets were released at about 10 chords upstream of the airfoil. The initial droplet velocity was set to the free-stream velocity at the far-field boundary. The results (in appendix D) show that greater number of droplet fragments was found in the coarser mesh (136,000 grid points) compared to the finer meshes (200,000 or 300,000 grid points). Droplet breakup also seemed to occur (relatively) further upstream and extended much further aft (of the LE of the airfoil) in the coarser mesh. The breakup process in the finer meshes exhibited greater consistency and repeatability. It is thought that the finer meshes produced more accurate pressure field, hence, more consistent droplet breakup. Details of this analysis are presented in appendix D, section D.1.

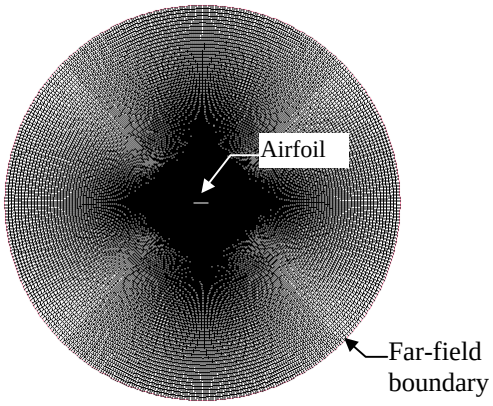

FIGURE 6-1b. COMPUTATIONAL GRID (NACA0012)

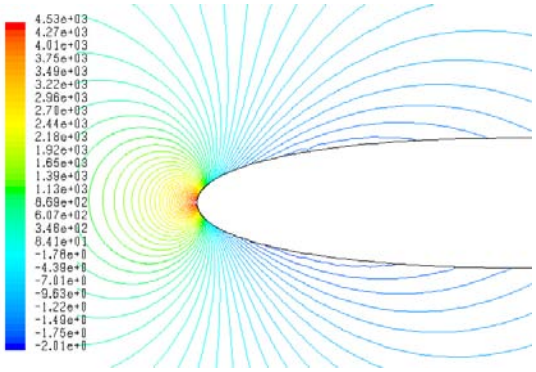

FIGURE 6-1c. PRESSURE CONTOUR AROUND THE NACA0012 AIRFOIL

To assess the effect of the droplet release location on breakup, droplets were released at 3 to 10 chords upstream of the airfoil. For each release location, the droplet velocity was set equal to the free-stream velocity at the grid outer boundary (i.e., 10 chord lengths from the airfoil). The computations were performed with the finer computational mesh of 300,000 grid points. The simulated results (appendix D, section D.2) showed that droplets released at locations less than 4 chord lengths upstream of the airfoil exhibited higher breakup densities (i.e., breakup was

observed at a large number of locations near the airfoil and these locations spanned a greater distance in the streamwise direction). Droplets that were released at locations further upstream of the airfoil (> 4 chords) exhibited greater consistency and repeatability. It is believed that the droplet relaxation time (i.e., the time required for a droplet to reach the free-stream velocity) was the main cause of this effect. Large droplets require longer relaxation times (hence, longer distances) to reach local free-stream velocity due to their greater inertias. Further details of this analysis can be found in appendix D, section D.2.

In summary, the analyses of the effects of grid resolution and initial droplet release location on the breakup process showed that the computational mesh appropriate for the current study should not have less than 200,000 points, and the droplet release location should be at least 5 chords ($x/c \geq 5$) away from the airfoil.

6.2 DROPLET BREAKUP NEAR A NACA0012 AIRFOIL.

Droplet breakup simulations were conducted with two NACA0012 airfoils having chord lengths of 3 and 20 ft. An O-type (2D) computational mesh with 200,000 points was created around each airfoil. The flow fields were computed with the FLUENT CFD software at the following conditions:

- Mach number of 0.3
- Zero angle of attack
- Altitude of 10,000 ft
- k-ε turbulence model
- Pressure far-field boundary

Figures 6-2 and 6-3 show pressure contours for the 3- and 20-ft chord airfoils respectively. The predicted pressure distributions (figures 6-2 and 6-3) in both cases are similar, i.e., regions of pressure gradients are concentrated near the stagnation area and aft of the LE of the airfoil. Droplet breakup was simulated in these flow fields using the following initial droplet conditions:

- Droplet diameters of 100, 500, and 1000 μm
- Droplet release location at 5-chord distant
- Droplet release velocity equal to free-stream velocity

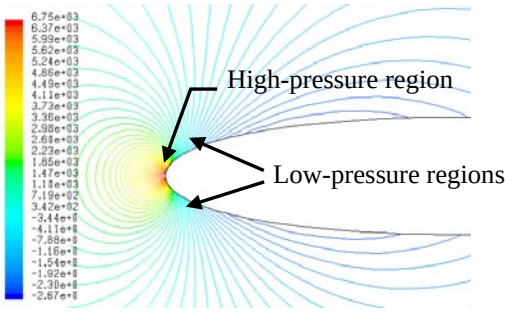

FIGURE 6-2. PRESSURE DISTRIBUTION FOR A 3-ft CHORD AIRFOIL, GAGE PRESSURE

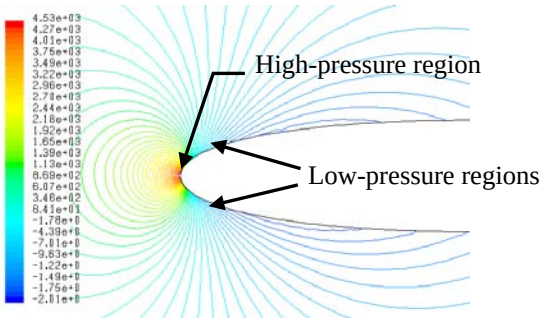

FIGURE 6-3. PRESSURE DISTRIBUTION FOR A 20-ft CHORD AIRFOIL

Figures 6-4a to 6-4c show the droplet sizes as they progressed toward the 3-ft airfoil for the initial droplet sizes of 100, 500, and 1000 μm respectively. Similarly, figures 6-5a to 6-5c show the droplet sizes in the 20-ft airfoil for the initial droplet sizes of 100, 500, and 1000 μm respectively. An assessment of the (droplet) breakup time and distance was carried out with the 20-ft airfoil and droplet diameter of 1000 μm only. The breakup time was computed using Pilch's correlations (section 3 and appendix C, section C.1). Figure 6-6 shows the distance traveled by the fragmented droplets (after breakup) prior to their impacts with the wall surface. Table 6-1 shows the computed breakup time and distance traveled by the fragmented droplets. The trajectory of each droplet in figure 6-6 is identified with a letter (A to E) that corresponds to the calculated value in table 6-1.

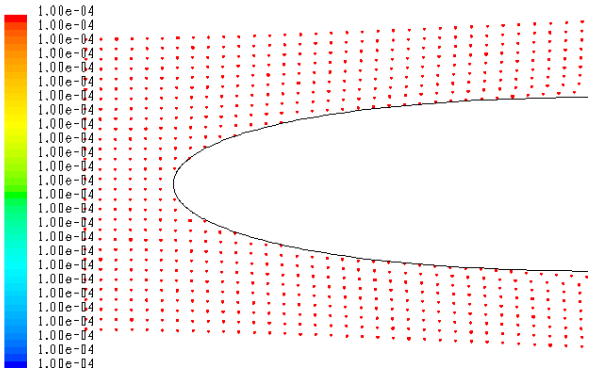

FIGURE 6-4a. DROPLET BREAKUP NEAR AIRFOIL, CHORD = 3 ft, D = 100 μm

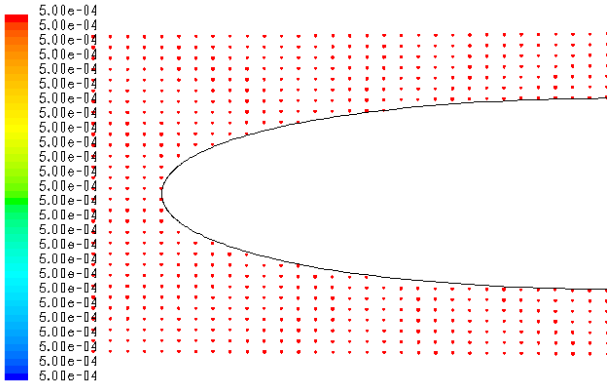

FIGURE 6-4b. DROPLET BREAKUP NEAR AIRFOIL, CHORD = 3 ft, D = 500 μm

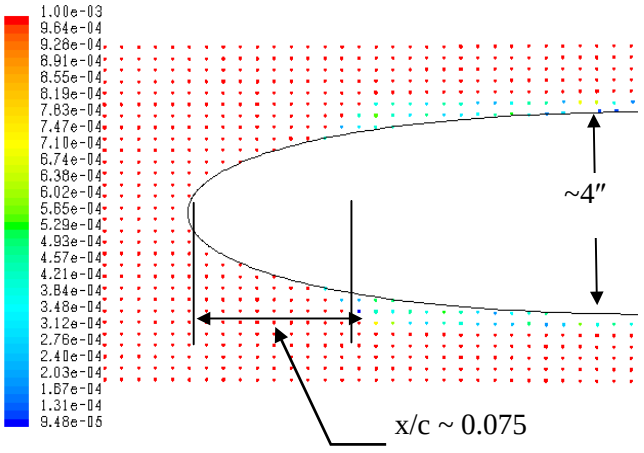

FIGURE 6-4c. DROPLET BREAKUP NEAR AIRFOIL, CHORD = 3 ft, D = 1000 μm

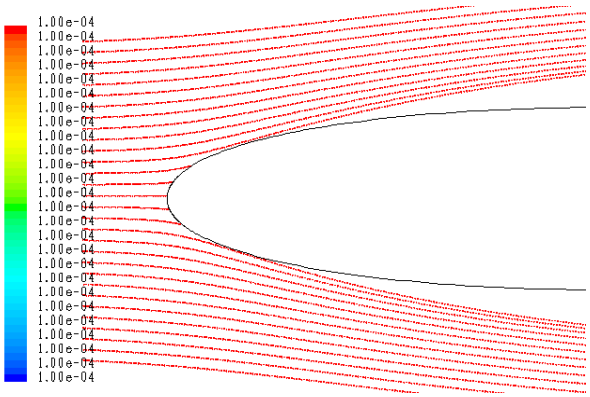

FIGURE 6-5a. DROPLET BREAKUP NEAR AIRFOIL, CHORD = 20 ft, D = 100 μm

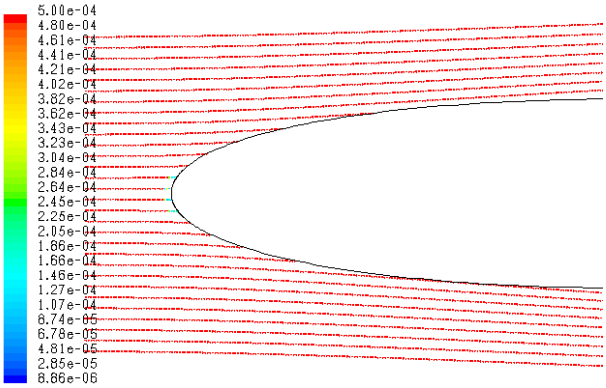

FIGURE 6-5b. DROPLET BREAKUP NEAR AIRFOIL, CHORD = 20 ft, D = 500 μm

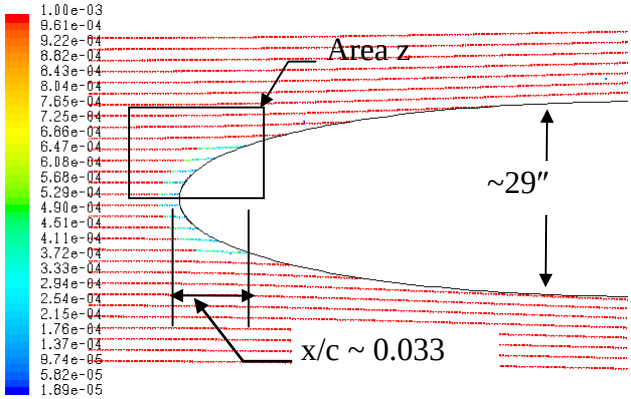

FIGURE 6-5c. DROPLET BREAKUP NEAR AIRFOIL, CHORD = 20 ft, D = 1000 μm

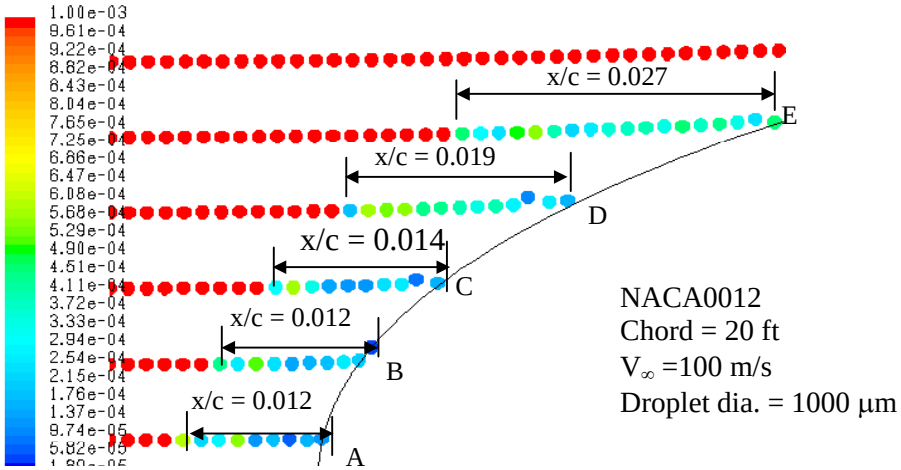

FIGURE 6-6. DROPLET BREAKUP LENGTH, CLOSE-UP VIEW OF AREA Z IN FIGURE 6-5c

TABLE 6-1. DROPLET BREAKUP TIMES AND DISTANCES, NACA0012 AIRFOIL, CHORD = 20 ft

Droplet Trajectory No.	Relative Droplet-Gas Velocity	Droplet Diameter	Weber Number	Breakup Time	Breakup Distance (Predicted)	Breakup Distance (Actual)
	(m/s)	(μm)		(s)	(x/c)	(x/c)
A	50.3	1000	33.09	0.003	0.053	0.012
B	45.0	1000	26.43	0.003	0.054	0.012
C	30.9	1000	12.37	0.008	0.127	0.014
D	15.6	1000	3.12	>0.008	>0.127	0.019
E	2.7	1000	0.09	>0.008	>0.127	0.027

6.3 RESULTS AND DISCUSSION (NACA0012 AIRFOIL).

For brevity, the discussion refers to the airfoil with a chord length of 3 ft as the 3-ft or smaller airfoil, and the 20-ft airfoil as the 20-ft or larger airfoil.

Figures 6-2 and 6-3 show similar predicted pressure distributions for the 3- and 20-ft airfoils. This is not unexpected since the initial and boundary conditions (e.g., altitude of 10,000 ft, Mach number of 0.3, etc.) for both airfoils were identical, and the only difference was their chord lengths. The pressure contours in both airfoils exhibited a high-pressure region near the LE of the airfoil, and low-pressure (upper and lower) regions immediately aft of the LE.

Figures 6-4a to 6-4c show droplet trajectories and sizes as the droplets progressed towards the 3-ft airfoil for initial droplet sizes of 100, 500, and 1000 μm respectively. Figures 6-5a to 6-5c show similar trajectory plots for the 20-ft airfoil. The simulations with the 100 μm droplets in both airfoils indicate no breakup, as demonstrated in figures 6-4a and 6-5a. However, the stronger aerodynamic forces in the case of the 20-ft airfoil (figure 6-5a) have greater effect on the droplet trajectories compared to those for the 3-ft airfoil case (figure 6-4a). Droplets near the larger airfoil were diverted further away from the airfoil surface aft of the LE compared to the displacement of droplets near the LE of the smaller airfoil. As the droplet sizes were increased to 500 μm, the effect of the aerodynamic forces on the trajectories was less pronounced; therefore, the trajectories were ballistic in nature, as shown in figures 6-4b and 6-5b for the small and large airfoils respectively. Some droplet breakups were observed near the stagnation region of the larger airfoil but none were found in the case of the smaller airfoil (500 μm case). Increasing droplet sizes from 500 to 1000 μm for the smaller airfoil did not promote breakup near the stagnation region but droplet breakups were found in the regions aft of the LE (upper and lower airfoil surfaces), as shown in figure 6-4c. In the case of the larger airfoil, greater breakup intensities were observed near the stagnation region only, as shown in figure 6-5c. These two different breakup behaviors for the small and large airfoils with the 1000 μm droplets can be explained by studying the free-stream pressures and velocities upstream of the airfoils (taken from their centerline locations), as shown in figures 6-7 and 6-8 respectively. Although the pressure and velocity values exhibited identical characteristics, the droplets residing in the locations upstream of the stagnation region of the 20-ft airfoil (e.g., at x/c = -0.2, hence, x = -4 ft) would be subjected to the effects of the high (negative) pressure gradients much earlier compared

to droplets at the same nondimensional axial locations of the 3-ft airfoil (e.g., x = -0.6 ft at x/c of -0.2). Droplet distortions, due to the effects of the pressure gradients, near the smaller airfoil would have occurred much closer to the airfoil, therefore, the droplets had insufficient time or distance to achieve the breakup stages. The breakup behaviors in the regions aft of the LE of the two airfoils (figures 6-4c and 6-5c) can be assessed by overlaying the breakup thresholds (limits of droplet breakup) with the wall static pressure distributions of the small and large airfoils, as shown in figures 6-9 and 6-10 respectively. Droplets traveling aft of the LE of the smaller airfoil (figure 6-9) exhibited breakup in the areas where x/c was greater than 0.075 since the breakup process was largely unimpeded. In contrast, droplet breakup for the larger airfoil (figure 6-10) was terminated beyond x/c of 0.033 since the pressure gradient in these regions (beyond x/c = 0.033) were low, therefore, no further breakup can be initiated.

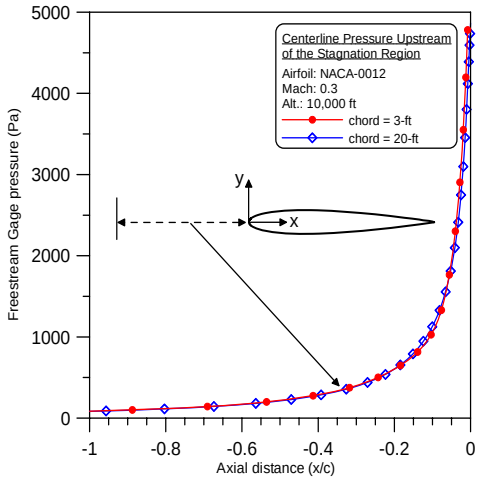

FIGURE 6-7. PRESSURE DISTRIBUTION ($P-P_\infty$) UPSTREAM OF NACA0012 AIRFOIL

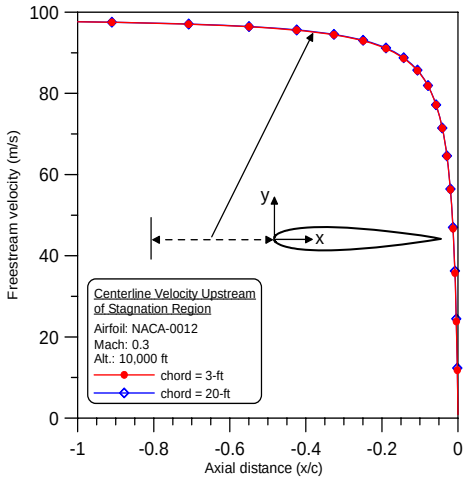

FIGURE 6-8. AIR VELOCITY DISTRIBUTION UPSTREAM OF NACA0012 AIRFOIL

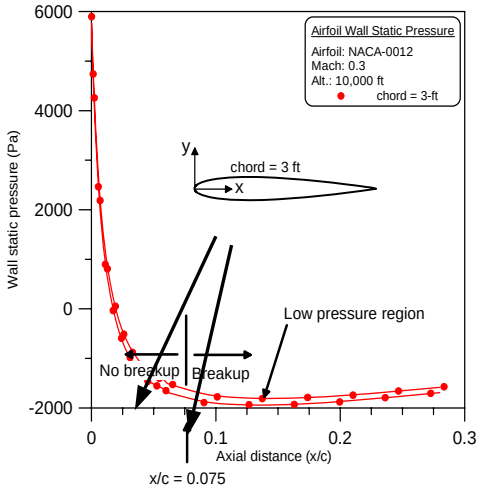

FIGURE 6-9. DROPLET BREAKUP AFT OF LE FOR THE 3-ft CHORD AIRFOIL

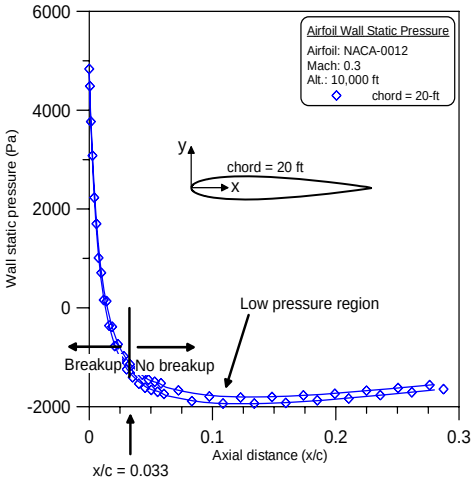

FIGURE 6-10. DROPLET BREAKUP AFT OF LE FOR THE 20-ft CHORD AIRFOIL

A limited analysis of the droplet breakup time was conducted with the 20-ft chord airfoil and a droplet diameter of 1000 μm in the highlighted area Z shown in figure 6-5c. The breakup time was computed using Pilch, et al.'s correlations [11], and the results are shown in table 6-1. Figure 6-6 shows the breakup distance traveled by the droplet. The required distance for achieving total breakup was calculated with the predicted total breakup time and velocity of the fragmented droplets (assumed equal to the droplet velocity prior to breakup). The results in table 6-1 show that all the droplets did not have sufficient distance to achieve complete breakup prior to impinging on the airfoil surface. However, it must be noted that previous validations of the TAB model with the vertical and horizontal tunnel (section 5.3) have shown that this model is capable of simulating vibrational and bag breakup modes only. No experimental data can be found to support these breakup modes since other modes such as shear or explosive may also occur in reality. However, the flow conditions under which droplet breakup occurred near the stagnation region and aft of the LE of the airfoil were similar to those found in the horizontal and vertical tunnels, where the validation of the TAB model was performed as shown in appendix E. Thus, it is believed that the TAB model is capable of predicting the breakup criteria (e.g., Weber and Rabin numbers) but not the type of breakup mode. If large droplet breakup occurs in practice, then future ice accretion codes would have to include a breakup model when simulating icing in SLD conditions. Current ice accretion codes assume that droplet breakup has no significant effect on the ice accretion process in 14 CFR Part 25, Appendix C icing conditions, although this has not been verified by experiments.

6.4 DROPLET BREAKUP NEAR A THREE-ELEMENT, HIGH-LIFT AIRFOIL.

The three-element airfoil [23 and 24] used in this study is representative of high-lift systems found in modern large transport aircraft and consisted of a slat, main, and flap elements as shown in figure 6-11a. The slat and flap deflection angles were set to the landing configuration: (slat) 30° LE down and (flap) 30° trailing edge (TE) down. To assess droplet breakup for large transport aircraft, a chord length of 20 ft was used. An O-type (2D) computational mesh was created around the airfoil with about 600,000 grid points. Local clustering of the grid points near the wall surfaces was applied to the slat, flap, and main elements as shown in figures 6-11b to 6-11d respectively. The computation of the flow field was carried out with the FLUENT code using the following conditions:

- Mach number of 0.3
- Zero AOA
- Altitude of 10,000 ft
- Spalart-Allmaras turbulence model
- Pressure far-field boundary placed at 10-chord lengths from the airfoil.

Figures 6-12a to 6-12c show the predicted pressure contours near the airfoil. Droplet breakup was computed in this flow field with the following droplet initial conditions:

- Droplet diameters of 100, 500, and 1000 μm
- Droplet release location at 5-chord distance
- Droplet release velocity equal to free-stream velocity

The droplet trajectories and breakup sizes for initial droplet diameter of 100, 500, and 1000 μm are shown in figures 6-13 to 6-15 respectively. Figures 6-16a through 6-18c show enlarged views of the droplet sizes near the slat, main, and flap elements.

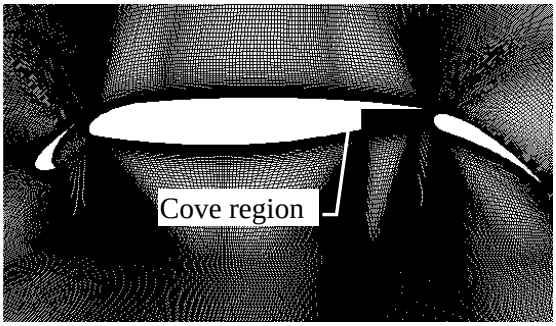

FIGURE 6-11a. COMPUTATIONAL GRID ON A THREE-ELEMENT AIRFOIL

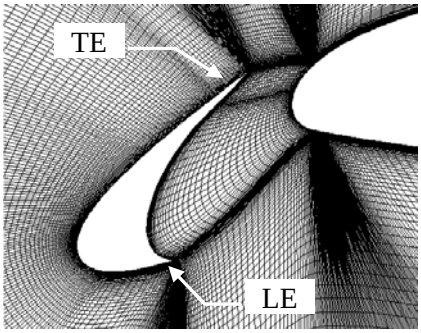

FIGURE 6-11b. NODE CLUSTERING ON THE SLAT ELEMENT

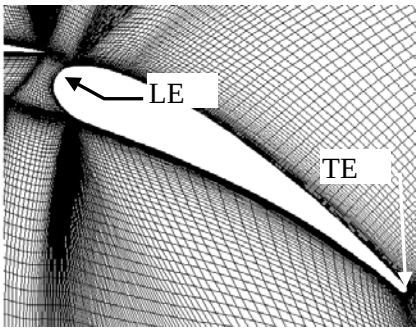

FIGURE 6-11c. NODE CLUSTERING ON THE FLAP ELEMENT

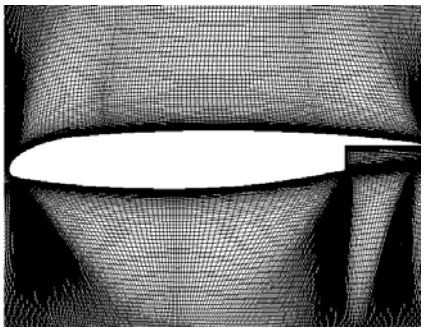

FIGURE 6-11d. NODE CLUSTERING ON THE MAIN ELEMENT

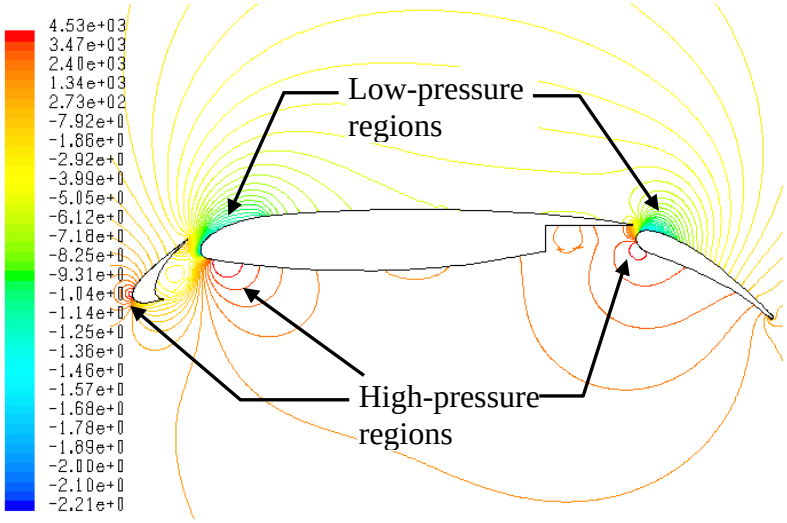

FIGURE 6-12a. PRESSURE DISTRIBUTION ON THE THREE-ELEMENT, HIGH-LIFT AIRFOIL

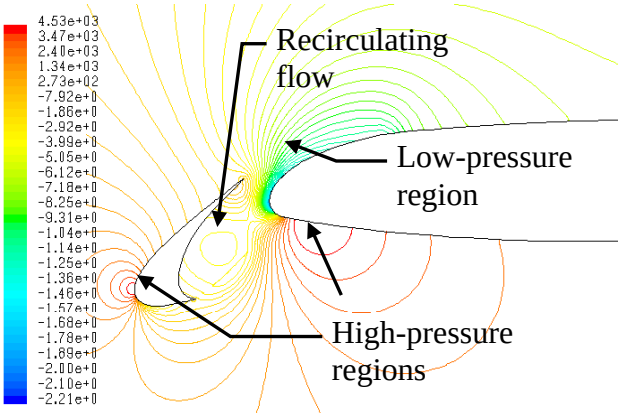

FIGURE 6-12b. PRESSURE DISTRIBUTION ON THE SLAT AND LE OF MAIN ELEMENT

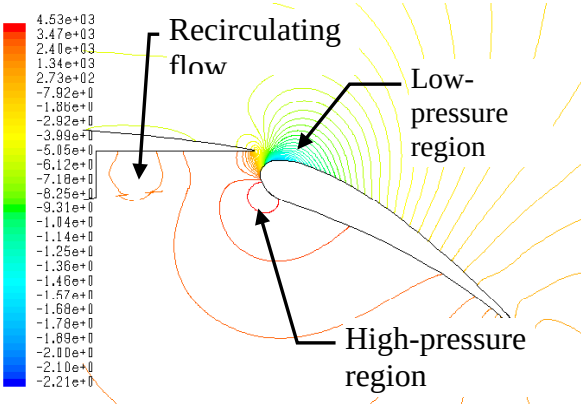

FIGURE 6-12c. PRESSURE DISTRIBUTION ON THE FLAP AND TE OF MAIN ELEMENT

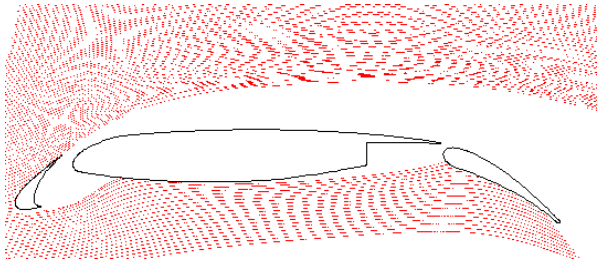

FIGURE 6-13. SIMULATION OF DROPLET BREAKUP, CHORD = 20 ft, D = 100 μm

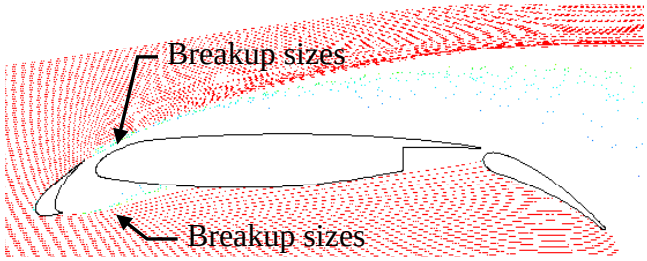

FIGURE 6-14. SIMULATION OF DROPLET BREAKUP, CHORD = 20 ft, D = 500 μm

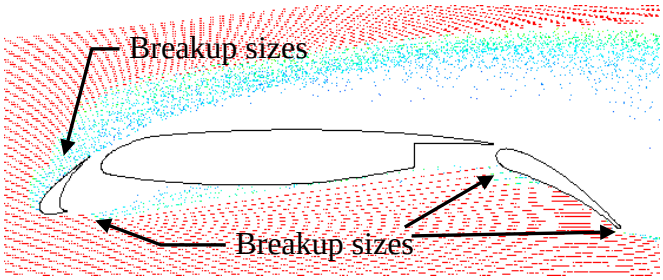

FIGURE 6-15. SIMULATION OF DROPLET BREAKUP, CHORD = 20 ft, D = 1000 μm

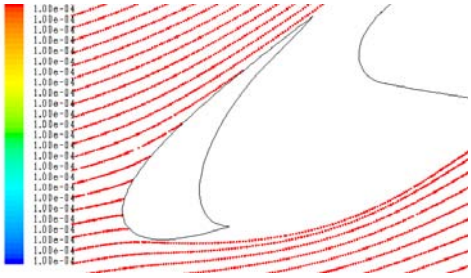

FIGURE 6-16a. DROPLET BREAKUP NEAR SLAT ELEMENT, D = 100 μm

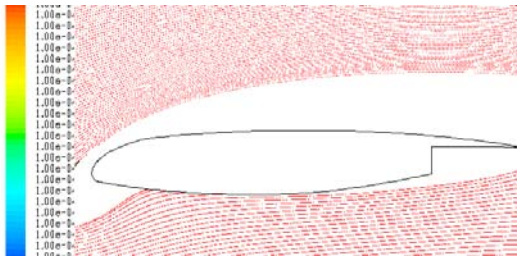

FIGURE 6-16b. DROPLET BREAKUP NEAR MAIN ELEMENT, D = 100 μm

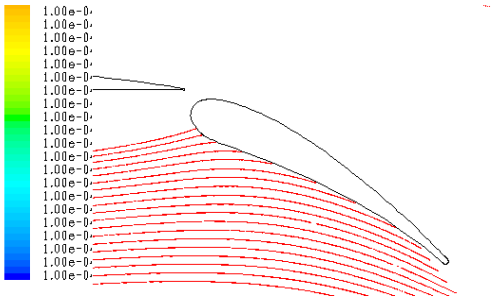

FIGURE 6-16c. DROPLET BREAKUP NEAR FLAP ELEMENT, D = 100 μm

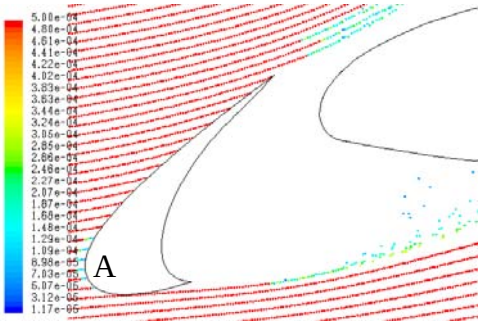

FIGURE 6-17a. DROPLET BREAKUP NEAR SLAT ELEMENT, D = 500 μm

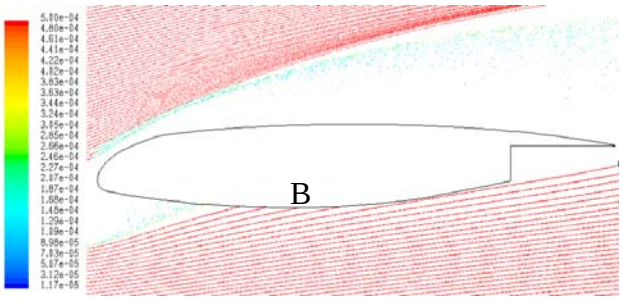

FIGURE 6-17b. DROPLET BREAKUP NEAR MAIN ELEMENT, D = 500 μm

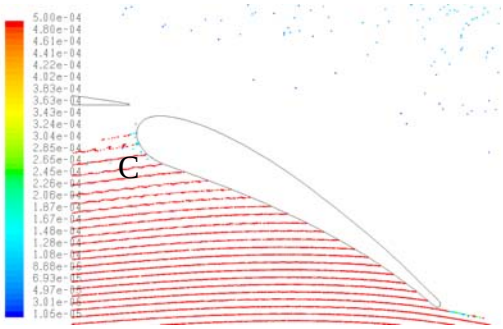

FIGURE 6-17c. DROPLET BREAKUP NEAR FLAP ELEMENT, D = 500 μm

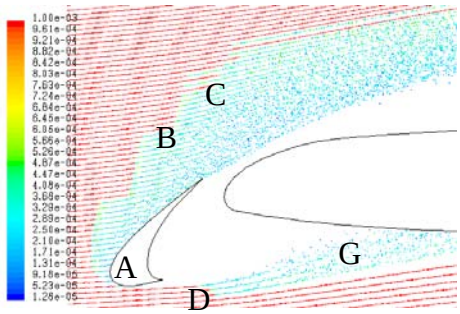

FIGURE 6-18a. DROPLET BREAKUP NEAR SLAT ELEMENT, D = 1000 μm

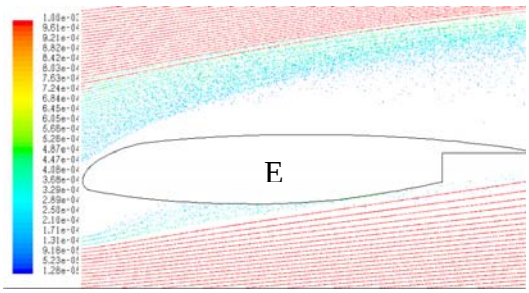

FIGURE 6-18b. DROPLET BREAKUP NEAR MAIN ELEMENT, D = 1000 μm

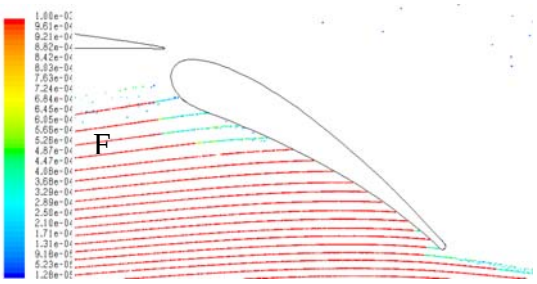

FIGURE 6-18c. DROPLET BREAKUP NEAR FLAP ELEMENT, D = 1000 μm

6.5 RESULTS AND DISCUSSION (THREE-ELEMENT AIRFOIL).

The computational results obtained with the NACA0012 airfoils showed that droplets generally breakup near regions with severe pressure gradients; therefore, similar trends would be expected in the case of the three-element airfoil. High- and low-pressure regions for the high-lift system are shown in figures 6-12a to 6-12c. A region of recirculating flow between the slat and main elements was observed in figure 6-12b and in the cove region of the main element (lower surface near the TE) as shown in figure 6-12c. Recirculating flows usually contain shear flow regions (shear layers) that can cause droplet breakup.

Figure 6-13 shows that no droplet breakup occurred with the 100-μm droplets. However, the trajectories of these droplets were diverted well away from the suction side (upper) of the main and flap elements by the aerodynamic forces. Droplet impingement occurred mainly at the frontal areas of the slat and on the pressure side (lower) of the main and flap elements. Figures 6-16a to 6-16c show enlarged views of the droplet impingement locations. As the initial droplet size increases to 500 μm, droplet breakup appeared downstream of the LE and TE of the slat element, as shown in figure 6-14. The fragmented droplets on the suction side passed harmlessly away from the airfoil without incurring any impacts in contrast to the droplet trajectories along the pressure side. Droplet impingement was observed on the pressure side of the main and flap elements (similar to those found for the 100-μm droplet case). Closer examination of the main element impingement characteristics (area B in figure 6-17b) shows that impingement started slightly further aft of the LE compared to the 100-μm case, as shown in figure 6-16b. It is believed that this is due to the stronger aerodynamic effects on the smaller fragmented droplets, and the greater inertias of those droplets that did not break up. Droplet breakup was found near

the high-pressure regions of the slat (area A) and flap (area C) elements, as shown in figures 6-17a and 6-17c respectively.

As the initial droplet diameter was increased to 1000 μm, more droplets experienced breakup, as shown in figure 6-15. Figure 6-18a shows that the droplet breakup area (upstream of the airfoil) extended from the stagnation region to the upper regions of the slat element (area A to C), which was significantly larger than the 500-μm droplets shown in figure 6-17a. Similar breakup behavior was also found in the aft regions of the slat (area D in figure 6-18a). There was no droplet impingement on the suction side of the main and flap elements, whereas impingement on the pressure side of the main element (area E, figure 6-18b) was due to fragmented droplets only. Droplet breakup was also found near the LE (area F) and TE (area G) of the flap element, as shown in figure 6-18c.

An assessment of the (droplet) breakup time (with Pilch, et al.'s correlations [11]) and distance was performed for the regions where droplet impingement (by fragmented droplets only) with the airfoil surface was found, and include the following regions:

a. Areas A and C for the 500-μm droplets in figures 6-17a and 6-17c respectively,
b. Areas A and F for the 1000-μm droplets in figures 6-18a and 6-18c respectively.

The computed results in table 6-2 shows the total breakup times and distances traveled by the fragmented droplets for cases (a) and (b) above. The results demonstrated that the distance between the location where droplet breakup occurred and the impingement location on the airfoil was not long enough to allow for complete droplet breakup to occur prior to impingement on the airfoil surface.

TABLE 6-2. DROPLET BREAKUP TIMES AND DISTANCES, THREE-ELEMENT AIRFOIL, CHORD = 20 ft

Droplet Trajectory No.	Relative Droplet-Gas Velocity (m/s)	Droplet Diameter (μm)	Weber Number	Breakup Time (sec)	Breakup Distance (Predicted) (x/c)	Breakup Distance (Actual) (x/c)
A	10.7-63.2	500	0.7-26.5	0.001-0.002	0015-0.030	0.004
C	5.6-53.7	500	0.2-18.7	>0.001	>0.011	0.003
A	20.7-46.1	1000	5.3-27.8	0.003-0.006	0.046-0.092	0.005-0.030
F	34.4-42.2	1000	15.5-23.4	0.004	0.050	0.019

In general, the droplet breakup analyses performed with the two NACA0012 airfoils and the three-element, high-lift system indicate the following:

- Droplet breakup occurred mainly in areas of the airfoils with severe pressure gradients, e.g., stagnation region, high- and low-pressure regions near LE and TE of airfoil.

- There were more occurrences of droplet breakup in the three-element airfoil (AOA = 0°) case compared to the NACA0012 airfoil (AOA = 0°) for the same droplet sizes and chord lengths.

- Where droplet breakup occurred close to the wall, e.g., stagnation regions, there was insufficient distance for the fragmented droplets to achieve complete breakup prior to their impingement on the airfoil.

- The droplet breakup studies with the two NACA0012 airfoils showed that droplet breakup for the 3-ft chord airfoil occurred aft of the LE, whereas for the 20-ft chord airfoil, breakup occurred at the stagnation region only.

- Larger droplets were more susceptible to droplet breakup than smaller droplets when they were subjected to similar aerodynamic forces.

- Aerodynamic forces had a significant effect on the trajectories of the small droplets. Trajectories of the larger droplets (≥ 500 μm) were generally ballistic in nature.

- Droplet breakup behavior depends on the droplet sizes, airfoil geometry (e.g., chord length, thickness-to-chord ratio, etc.), airfoil type (e.g., single airfoil and multielement airfoil, etc.), and configurations (e.g., AOA, flap and slat settings, etc.).

7. SUMMARY.

A literature review of droplet breakup studies and 2D simulations of small and large droplet breakup in the proximity of airfoils were performed. The findings of the literature review indicate that the critical Weber number for characterizing droplet breakup can vary, depending on the experimental test facility and relative droplet-air velocity, e.g., *We* ~13 in shock tube, *We* ~22 in free-fall. Droplets will also undergo multistage breakup as long as the fragment sizes continue to exceed critical values. The breakup time consists of the initiation (deformation) and primary breakup times, and the total breakup time is defined as the time required for complete disintegration of a droplet.

Droplet breakup simulation was carried out with the TAB model, which resides within the FLUENT computational fluid dynamics software. Limited validation of the TAB model was conducted with experimental data collated in horizontal and vertical tunnels. The numerical predictions of droplet breakup were found to be in good correlation with the experimental results for the validation cases selected. The predicted critical Weber numbers ($9.4 < We < 16.0$) in the horizontal tunnel generally showed good agreement with the measured values ($13.7 < We < 14.07$). For the vertical tunnel validation case, the predicted Rabin numbers ($0.4 < Ra < 0.5$) also showed good agreement with the experimental data ($0.36 < Ra < 0.47$) at a tunnel velocity of 150 ft/s. However, at higher tunnel velocities (> 150 ft/s), the predicted Rabin numbers ($0.3 < Ra < 0.6$) were generally lower than the experimental data ($0.7 < Ra < 0.9$). It is believed that at higher tunnel velocities, the shear breakup mode was predominant, and the TAB model is limited to vibrational and bag breakup modes in the current application.

The effects of the grid resolution of the computational mesh and initial droplet release location on breakup were also investigated. It was found that coarser computational mesh and droplets that were released too close to the airfoil tended to promote earlier droplet breakup, hence, overprediction of the breakup behavior. The knowledge gained from this sensitivity study was applied to two NACA0012 airfoils with chord lengths of 3 and 20 ft and a three-element airfoil with a chord length of 20 ft. The slat and flap elements of the three-element airfoil was set to represent the landing configuration, i.e., 30° LE (slat) and TE down (flap). The simulation conditions used were representative of an aircraft operating at 10,000 ft and Mach number of 0.3. Monodispersed droplets with diameters of 100, 500, and 1000 μm were released at a distance of 5-chord lengths upstream of the airfoil. These droplet sizes represent the maximum droplet size in 14 CFR Part 25, Appendix C cloud, threshold size for freezing drizzle and rain, and the maximum droplet size applicable to the TAB model (for the current study) respectively. A summary of key findings from the study conducted is provided below.

- Droplets of 100 μm diameter did not experience breakup near the NACA0012 or three-element airfoils.

- Droplets of 500 μm diameter exhibited breakup near the stagnation region of the 20-ft chord NACA0012 and three-element airfoils, but no breakup was observed for the 3-ft chord NACA0012 airfoil case. Additional breakup was also found aft of the LE and TE of the slat element in the three-element airfoil.

- Droplet breakup was found in all three airfoils for droplets with diameters of 1000 μm. Major differences in the regions where breakup occurred were found for the 3- and 20-ft NACA0012 airfoils. For the 3-ft airfoil, droplet breakup occurred in the regions aft of the LE, whereas for the 20-ft airfoil, breakup occurred only near the stagnation region. In the case of the three-element airfoil, droplet breakup (with a droplet diameter of 1000 μm) extended over wide regions upstream and downstream of the LE of the slat element. Extensive breakup was also found in the stagnation region and aft of the flap element. Droplet impingement by the fragmented droplets was observed mainly on the pressure side (lower surface) of the main and flap elements but not on the suction side (upper surface). The slat element incurred droplet breakup and impingement on the frontal area only.

- Aerodynamic forces had a significant effect on the trajectories of the smaller 100 μm droplets for all the airfoils. Trajectories of the larger droplets (≥ 500 μm) were ballistic in nature for the two NACA0012 airfoils tested (AOA = 0°). For the three-element airfoil however, the trajectories of the 500- and 1000-μm droplets experienced greater deflections in away from the airfoil compared to the NACA 0012 airfoil.

- Analyses of the droplet breakup time and distances conducted with the 20-ft NACA0012 airfoil and the three-element, high-lift system showed that droplets generally did not have sufficient distance to achieve complete breakup before impinging on the airfoil surface.

Finally, some considerations on droplet breakup modeling:

- Droplet breakup affects mainly SLD icing conditions due to the greater number of large droplets found in SLD clouds. It is not known if droplet breakup would have a significant effect on icing in 14 CFR Part 25, Appendix C clouds.

- For clean airfoils, droplet breakup depends on the airfoil type (e.g., single, two- or three-elements, etc.), chord length, configuration (e.g., AOA, flap, and slat in extended or stowed position, etc.), operating conditions (e.g., speed, altitude) and droplet sizes.

- For iced airfoils, regions with adverse pressure gradients, e.g., behind ice ridges, would be more likely to cause droplet breakup irrespective of airfoil type or configuration due to the effects of the shear flow and boundary layers.

- The effect of droplet breakup on ice scaling laws is unknown but geometrically similar airfoils with different chord lengths can exhibit different breakup behavior.

In the current study, the breakup modes that were simulated with the TAB model are limited to vibrational and bag modes. It is not known whether droplet breakup near an airfoil would exhibit these or other breakup modes since no experimental data can be found in published literature. However, the flow-field conditions under which droplet breakup occurred near the stagnation region and aft of the LE of the airfoil were similar to the flow fields in the horizontal and vertical tunnel experiments used to validate the TAB model. Thus, it is believed that this model is capable of predicting droplet breakup criteria (e.g., Weber and Rabin numbers) but not the type of breakup mode. Note that different breakup modes produce different breakup

(fragmented) sizes (e.g., vibrational breakups usually produce several droplets that are comparable to the initial droplet sizes, whereas bag and shear modes usually produce a large distribution of smaller droplets). Since larger breakup droplet sizes are less influenced by the aerodynamic forces compared to smaller breakup droplet sizes, the droplet impingement characteristics on an airfoil undergoing large droplet breakup will be a function of the size of the resulting droplet fragments.

The numerical analysis has shown that the TAB model is capable of simulating vibrational and bag types of breakup only. It is not known whether these breakup modes occur in practice. However, it is believed that regions with severe pressure gradients are deemed likely to cause droplet breakup, e.g., stagnation, high- and low-pressure regions. It is, therefore, recommended that experimental tests be conducted to assess the following effects on droplet breakup and breakup modes:

- The effects of pressure gradient.
- The effects of relative droplet-gas velocity.
- The effects of absolute pressure forces.
- The effects of droplet sizes after breakup.

Whatever test facility is employed in any future study, it should be able to provide variable pressure gradient and relative droplet-gas velocity. Test equipment and instrumentation such as a monodispersed droplet generator, high-speed imaging system, droplet-sizing instrument, and pressure measurement devices would also be required.

8. REFERENCES.

1. Cober, S.G., Isaac, G., Shah, A.D., and Jeck, R., "Defining Characteristic Cloud Droplet Spectra from In-situ Measurements," AIAA, 2003-0561.

2. Lane, W.R., "Shatter of Drops in Stream of Air," *Ind. Eng. Chem.*, 43, No. 4, 1951, pp. 1312-1317.

3. Lane, W.R., Prewett, W.C., and Edwards, J., "Some Experiments on the Shatter of Drops by Transient Blast of Air," Tech. Paper No.115, Serial 15, Porton, England, 1949.

4. Lane, W.R. and Dorman, R.G., "Further Experiments on the Shattering of Drops by a Supersonic Air Blast," Tech. Paper No., 279, Porton, England, 1952.

5. Hinze, J.O., "Fundamentals of the Hydrodynamic Mechanism of Splitting in Dispersion Processes," *A.I.Ch.E. Journal*, Vol. 1, No. 3, 1955, pp. 289-295.

6. Hinze, J.O., "Critical Speeds and Sizes of Liquid Globules," *Applied Scientific Research*, A1, 1949, pp. 273-288.

7. Wolfe, H.E. and Andersen, W.H., "Kinetics, Mechanism, and Resultant Droplet Sizes of the Aerodynamic Breakup of Liquid Drops," Aerojet-General Corporation Research and Engineering Division Report No. 0395-04 (18)SP, 1964.

8. Simpkins, P.G. and Bales, L., "Water-Drop Response to Sudden Acceleration," *J. Fluid Mech*., Vol. 55, Part 4, 1972.

9. Borisov, A.A., "Droplet Breakup Regimes and Criteria for their Existence," *J. Eng. Physics*, 40, 1,1981.

10. Krzeczkowski, S.A., "Measurement of Liquid Droplet Disintegration Mechanism," *Int. J. Multiphase Flow*, Vol. 6, 1980, pp. 227-239.

11. Pilch, M. and Erdman, C.A., "Use of Breakup Time Data and Velocity History Data to Predict the Maximum Size of Stable Fragments for Acceleration-Induced Breakup of a Liquid Drop," *Int. J. Multiphase Flow*, 13, No. 6, 1987, pp. 741-757.

12. Wierzba, A., "Deformation and Breakup of Liquid Drops in a Gas Stream at Nearly Critical Weber Numbers," *Experiments in Fluids* 9, 1990, pp. 59-64.

13. Hirahara, H. and Kawahashi, M., "Experimental Investigation of Viscous Effects Upon a Breakup of Droplets in High Speed Airflow," *Experiment in Fluids*, 13, 1992, pp. 423-428.

14. Kennedy, J.B. and Roberts, J., "Rain Ingestion in a Gas Turbine Engine," ILASS-AMERICAS, Inst. of Liquid Atomization and Spray Systems, 4th Annual Conference, Hartford, CT, USA, 1990, pp. 154-186.

15. Suzuki T. and Mitachi, K., "Experimental Study on Aerodynamic Breakup of Liquid Droplets in Time-Dependent Relative Velocity Fields," *8th Int. Conf. Liquid Atomization and Spray Systems*, Pasadena, CA, July 2000.

16. Reitz, R.D. and Diwakar, R., "Structure of High-Pressure Fuel Spray," SAE Technical Paper Series 870598.

17. Hsiang, L.P. and Faeth, G.M., "Near Limit Drop Deformation and Secondary Breakup," *Int. J. of Multiphase Flow*, 18(5), 1992.

18. Rabin, E.A., Schallenmuller, A.R., and Lawhead, R.B., "Displacement and Shattering of Propellant Droplet," Final Summary Report, Washington DC, U.S. Airforce, Office of Scientific Research, AFOSR TR 60-75, March 1960.

19. O'Rouke, P.J. and Amsden, A.A., "The TAB Method for Numerical Calculation of Spray Droplet Breakup," SAE Paper 87-2089, 1987.

20. Reitz, R.D. "Mechanism of Atomization Processes in High Pressure Vaporizing Spray," *Atomization and Spray Technology*, Vol. 3, 1987, pp. 309-337.

21. Reitz, R.D. and Bracco, F.V., "Mechanism of Atomization a Liquid Jet," *Physics of Fluids*, 26(10), 1982.

22. Hiroyasu, H. and Kadota, T., "Fuel Droplet Size Distribution in Diesel Combustion Chamber," SAE paper 740715, 1974.

23. Valarezo, W.O., Dominik, C.J., McGhee, R.J., Goodman, W.L., and Paschal, K.B., "Multi-Element Airfoil Optimization for Maximum Lift at High Reynolds Numbers," AIAA-91-3332, September 1991.

24. Valarezo, W.O., Dominik, C.J., and McGhee, R.J., "Reynolds and Mach Number Effects on Multi-Element Airfoils," *Fifth Symposium on Numerical and Physical Aspects of Aerodynamic Flows*, Long Beach, CA, January 1992.

APPENDIX A—NONDIMENSIONAL GROUPS

The behavior of a droplet subjected to a gas flow can be defined with the following nondimensional groups (used throughout this report):

1. Reynold number (*Re*)

$$Re = \frac{\rho_g |V_d - V_g| D}{\mu_g} = \frac{\rho_g |V_r| D}{\mu_g}$$

2. Weber number (*We*)

$$We = \frac{\rho_g |V_r|^2 D}{\sigma_d}$$

3. Ohnesorge number (*Oh*)

$$Oh = \frac{\mu_d}{\sqrt{\rho_d D \sigma_d}}$$

4. Laplace number (*La*)

$$La = \frac{1}{Oh^2}$$

5. Bond number (*Bo*)

$$Bo = \frac{\rho_d D^2}{\sigma_d}\left(\frac{dV_r}{dt}\right)$$

6. Rabin number (*Ra*)

$$Ra = We/\sqrt{(Re)}$$

APPENDIX B—PREVIOUS DROPLET BREAKUP STUDIES—TEST FACILITIES AND RESULTS

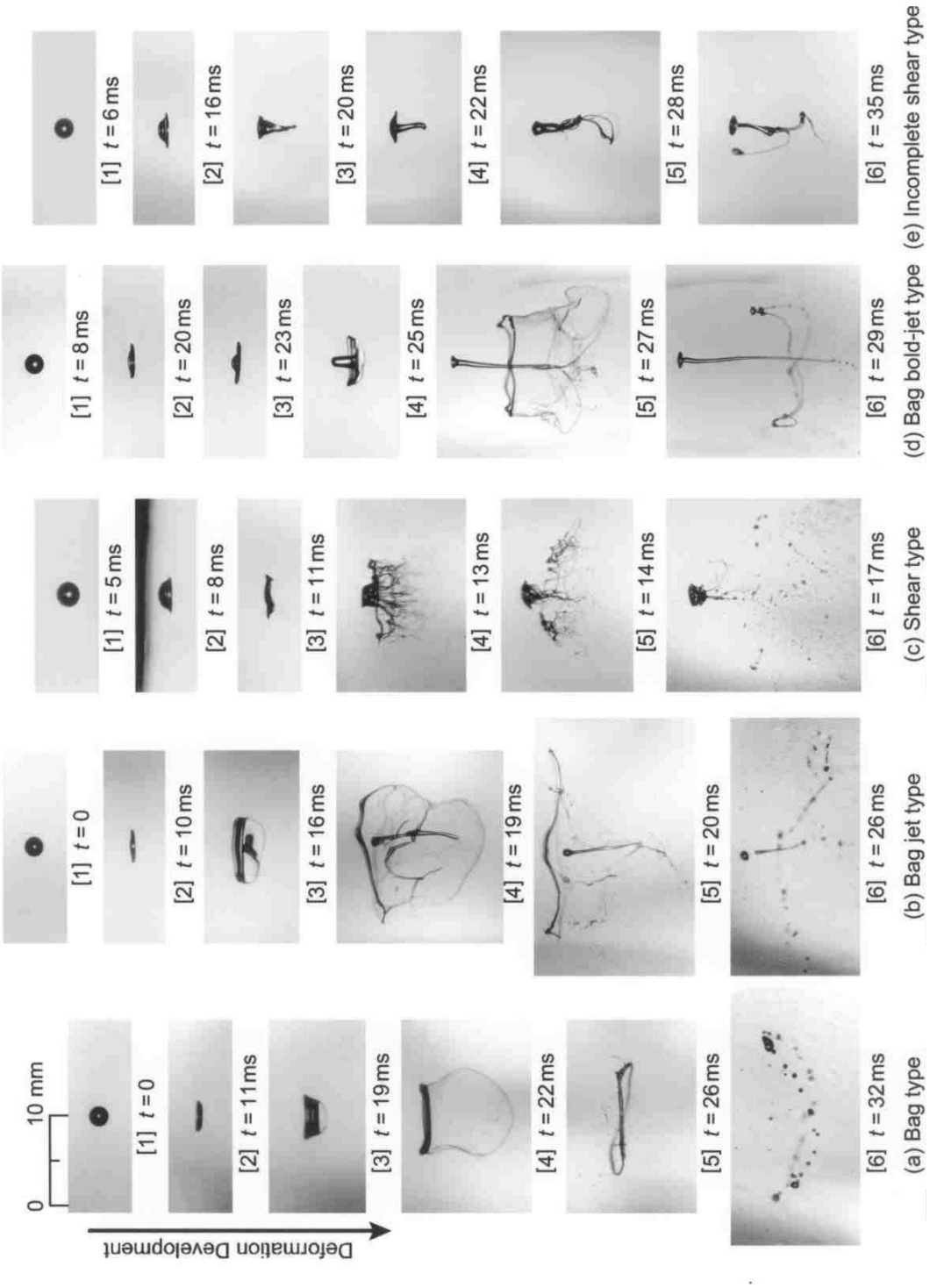

FIGURE B-1. DROPLET BREAKUP MODES AND TIMES OF SILICON OIL (Courtesy of Suzuki, et al. [B-1])

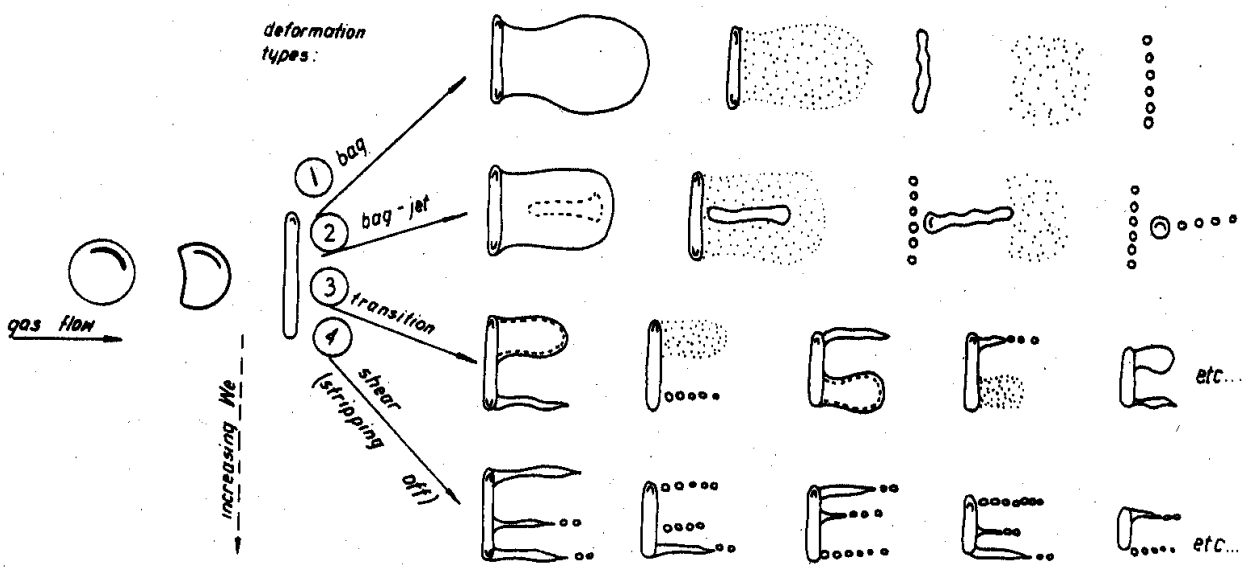

FIGURE B-2. ILLUSTRATION OF DROPLET TRANSITIONS (from Krzeczkowski [B-2])

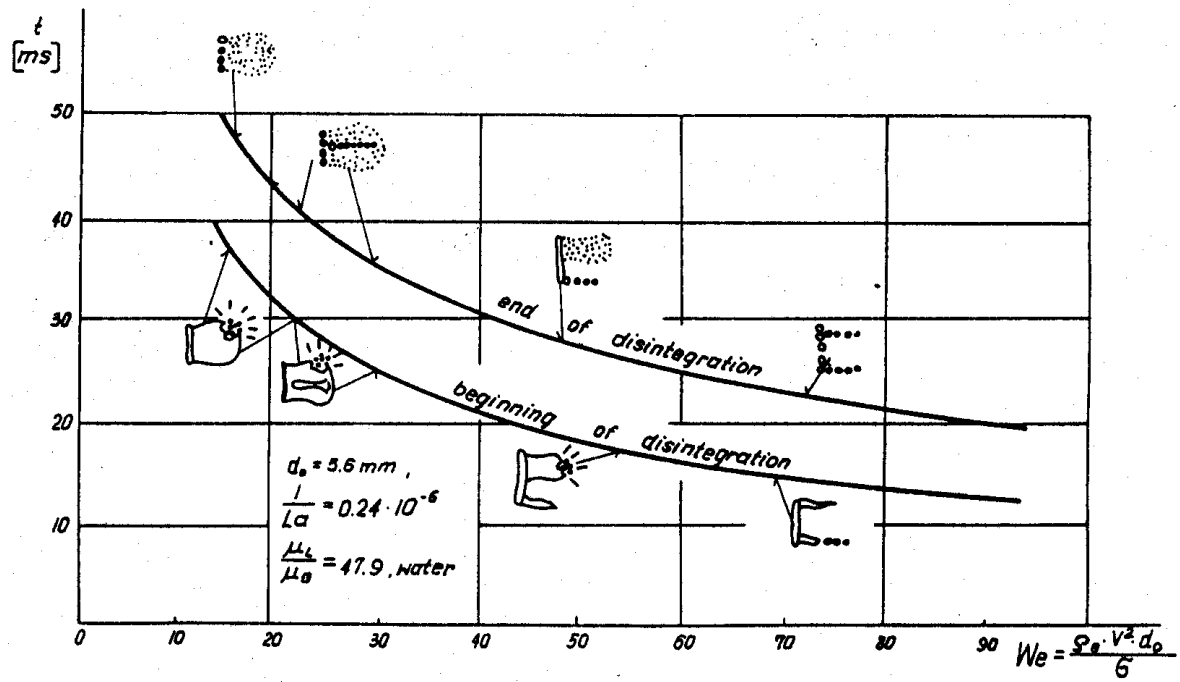

Break-up duration vs the Weber Number for water droplets (beginning and the end of disintegration).

FIGURE B-3. DROPLET BREAKUP TIMES, BEGINNING AND END OF DISINTEGRATION (from Krzeczkowski [B-2])

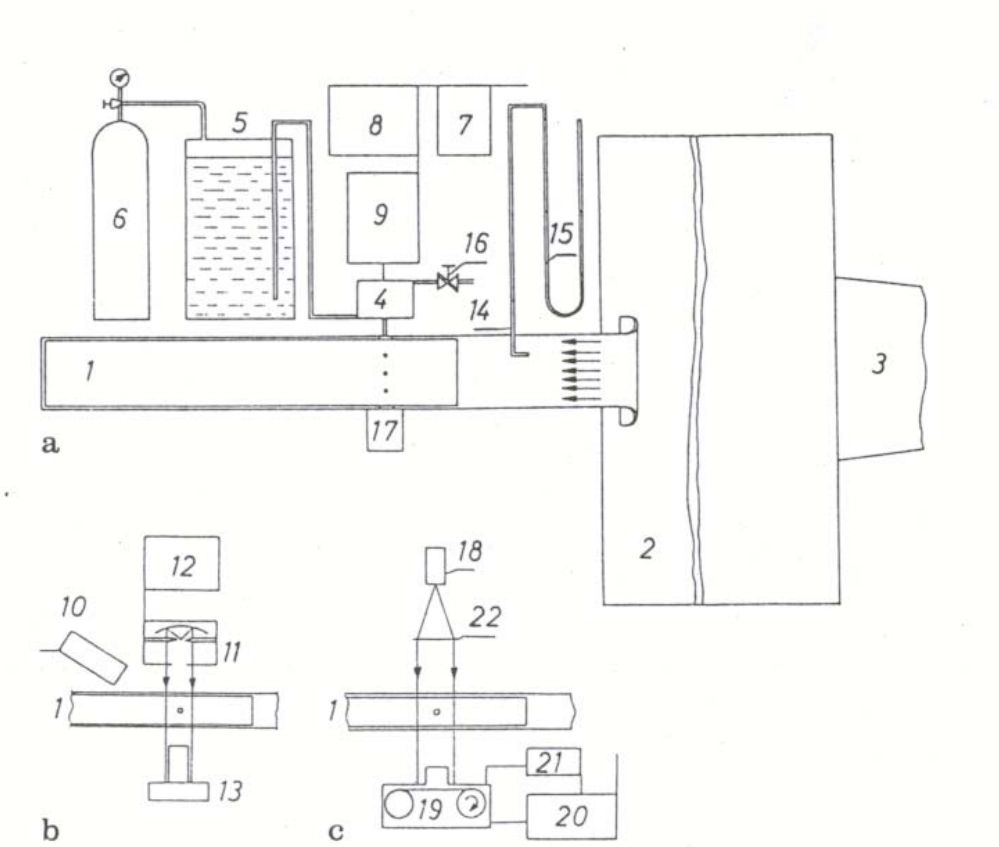

Fig. 1 a–c. Schematic diagram of experimental arrangement; *1* – test section, *2* – air reservoir, *3* – diffuser, *4* – droplet generator, *5* – distilled water tank, *6* – gas bottle, *7* – variable frequency signal generator, *8* – amplifier, *9* – vibrator, *10* – stroboscopic lamp, *11* – spark light source, *12* – trigger generator, *13* – photocamera, *14* – Pitot tube, *15* – micromanometer, *16* – air bleed valve, *17* – droplet catch system, *18* – mercury lamp, *19* – high speed movie camera, *20* – camera control unit, *21* – time signal generator, *22* – lens

FIGURE B-4. HORIZONTAL TUNNEL FOR STUDYING DROPLET BREAKUP
(from Wierzba [B-3])

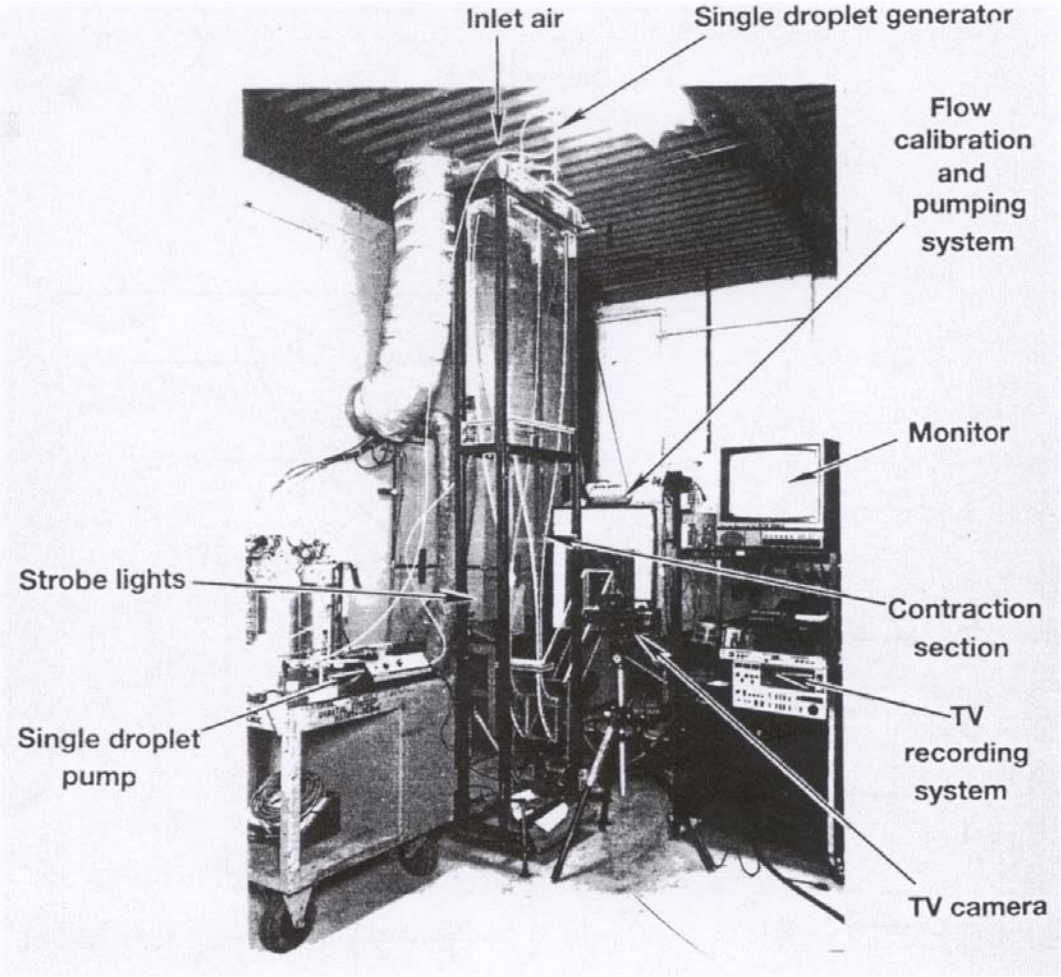

FIGURE B-5. VERTICAL TUNNEL FOR STUDYING DROPLET BREAKUP (from Kennedy, et al. [B-4])

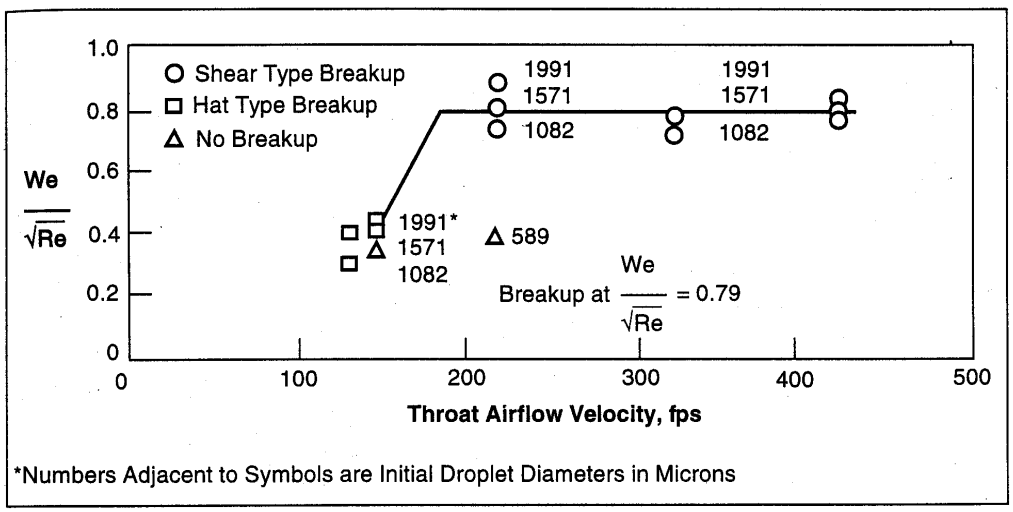

FIGURE B-6. DROPLET BREAKUP MODES (from Kennedy, et al. [B-4])

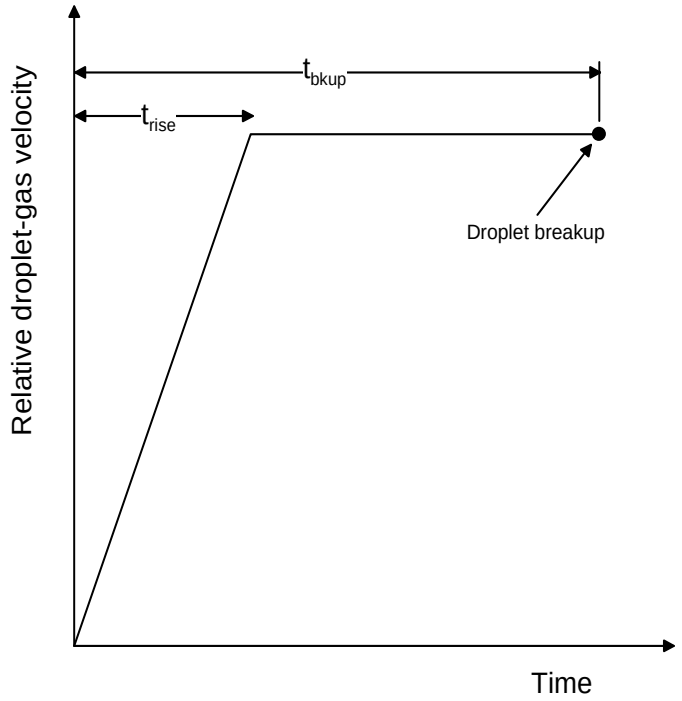

FIGURE B-7. CASE (I) DROPLET-GAS VELOCITY RISE TO A SETTLING VALUE WITHIN A FINITE TIME (courtesy of Suzuki, et al. [B-1])

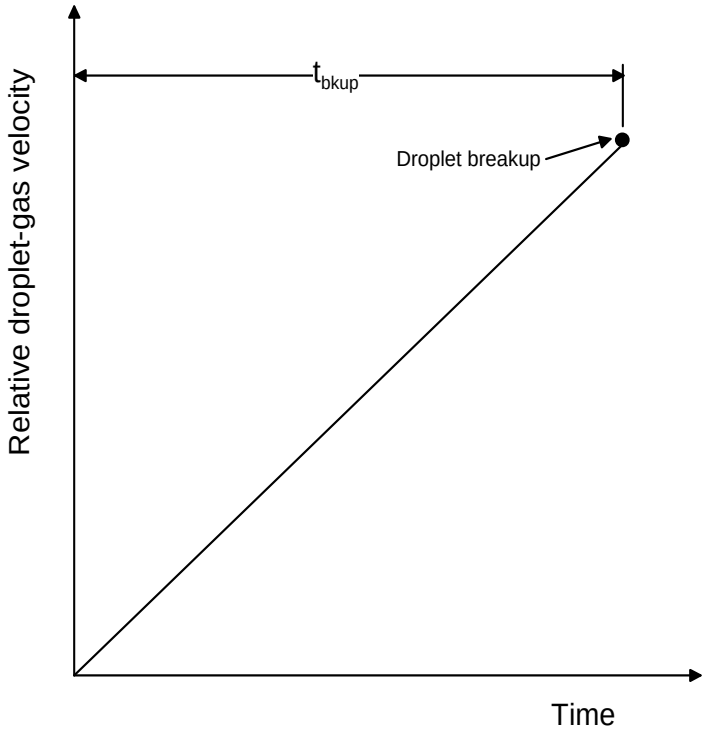

FIGURE B-8. CASE (II) DROPLET-GAS VELOCITY INCREASES LINEARLY WITH TIME (courtesy of Suzuki, et al. [B-1])

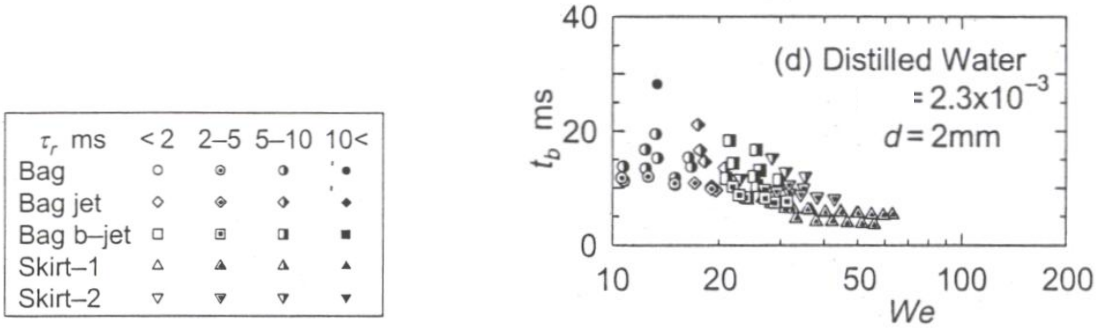

FIGURE B-9. CASE (I) DROPLET BREAKUP TIME IN THE CASE WHERE DROPLET-GAS VELOCITY RISE TO A SETTLING VALUE WITHIN A FINITE TIME (courtesy of Suzuki, et al. [B-1])

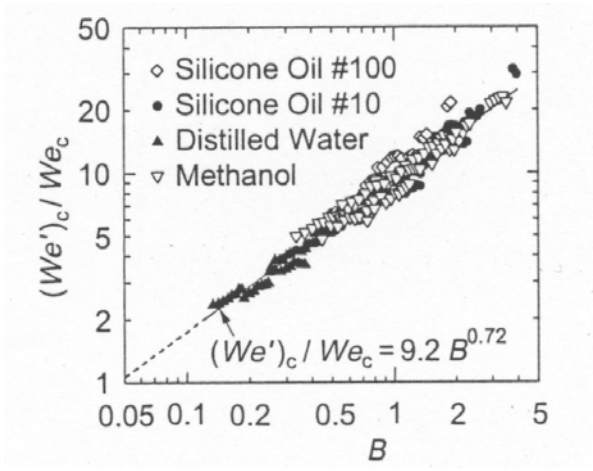

FIGURE B-10. CASE (II) RATIO OF CRITICAL WEBER NUMBER IN CASE (II) TO THE CRITICAL VALUE MEASURED IN CASE (I) (courtesy of Suzuki, et al. [B-1])

REFERENCES.

B-1. Suzuki T. and Mitachi, K., "Experimental Study on Aerodynamic Breakup of Liquid Droplets in Time-Dependent Relative Velocity Fields," *8th Int. Conf. Liquid Atomization and Spray Systems*, Pasadena, CA, July 2000.

B-2. Krzeczkowski, S.A., "Measurement of Liquid Droplet Disintegration Mechanism," *Int. J. Multiphase Flow*, Vol. 6, 1980, pp. 227-239.

B-3. Wierzba, A., "Deformation and Breakup of Liquid Drops in a Gas Stream at Nearly Critical Weber Numbers," *Experiments in Fluids* 9, 1990, pp. 59-64.

B-4. Kennedy, J.B. and Roberts, J., "Rain Ingestion in a Gas Turbine Engine," ILASS-AMERICAS, Inst. of Liquid Atomization and Spray Systems, 4th Annual Conference, Hartford, CT, USA, 1990, pp. 154-186.

APPENDIX C—DROPLET BREAKUP MODELS

C.1 STAR-CD.

C.1.1 REITZ AND DIWAKER MODEL [C-1].

The bag type breakup criterion is defined by the Weber number:

$$We = \frac{\rho_g \cdot \left| v_g - v_d \right| \cdot D}{\sigma_d} \geq C_{b1}$$

The associated breakup time is

$$\tau_b = \frac{C_{b2} \cdot (\rho_d)^{\frac{1}{2}} \cdot D^{\frac{3}{2}}}{4 \cdot (\sigma_d)^{\frac{1}{2}}}$$

C_{b1} can have values between 7.2 and 16.8 but STAR-CD uses $C_{b1} = 12$ and $C_{b2} \approx \pi$.

The stripping (or shear) type breakup is defined with the Rabin number (*Ra*):

$$\left(Ra = \frac{We}{\sqrt{\mathrm{Re}_D}} \right) \geq C_{s1}$$

The droplet breakup time is

$$\tau_b = \frac{C_{s2} \cdot D}{2 \cdot \left| v_g - v_d \right|} \cdot \left(\frac{\rho_d}{\rho_g} \right)^{\frac{1}{2}}$$

$C_{s1} = 0.5$, C_{s1} can have values between 2 and 20 but STAR-CD uses $C_{s1} = 20$. No equation is given for the stable droplet diameter (after breakup). The stable droplet diameter, D_s, is that which satisfies the following equation:

$$\frac{\rho_g \cdot \left| v_g - v_d \right| \cdot D_s}{\sigma_d} = 12$$

C.1.2 PILCH AND ERDMAN MODEL [C-2].

Critical breakup values and times are characterized by five distinct modes:

- vibrational breakup: $12 \leq We \leq 18$, $T = 6.0(We\text{-}12)^{-0.25}$
- bag breakup: $18 \leq We \leq 45$, $T = 2.45(We\text{-}12)^{0.25}$
- bag and stamen breakup: $45 \leq We \leq 351$, $T = 14.1(We\text{-}12)^{-0.25}$

- sheet stripping: $351 \le We \le 2670$, $T = 0.766(We\text{-}12)^{0.25}$
- wave crest stripping: $We > 2670$, $T = 5.5$

where

$$We = 12\left[1 + 1.077\left(Oh\right)^{1.6}\right]$$

and

$$\tau_b = T \cdot \left[\frac{D}{\left|v_g - v_d\right|} \cdot \left(\frac{\rho_d}{\rho_g}\right)^{\frac{1}{2}}\right]$$

The maximum stable droplet diameter after breakup is

$$d_{\max} = We\frac{\sigma_d}{\rho_g V_r^2}\left(1 - \frac{V_{frag}}{V_r}\right)^{-2}$$

where

$$v_{frag} = \left|v_g - v_d\right| \cdot \left(\frac{\rho_g}{\rho_d}\right)^{\frac{1}{2}} \cdot \left(B_1 \cdot T + B_2 \cdot T^2\right)$$

and $B_1 = 0.375$ and $B_2 = 0.2274$.

C.1.3 Hsiang and Faeth model [C-3].

Droplet breakup takes place if

$$We = \frac{\rho_g \cdot \left|v_g - v_d\right| \cdot D}{\sigma_d} \ge 12$$

The droplet breakup time is

$$\tau_b = \frac{5 \cdot D}{\left[1 - \left(\frac{Oh}{7}\right)\right] \cdot \left|v_g - v_d\right|} \cdot \left(\frac{\rho_d}{\rho_g}\right)^{\frac{1}{2}}$$

The maximum stable droplet diameter after breakup is

$$d_{\max} = 6.2 \cdot D \cdot \left(\frac{\rho_d}{\rho_g} \right)^{\frac{1}{4}} \cdot \sqrt{\frac{\mu_d}{D \cdot \rho_d \cdot \left| v_g - v_d \right|}}$$

The drag coefficient for a perfect sphere is

$$C_D = \begin{cases} \left| \frac{24}{Re} \left(1 + 0.15 \cdot Re^{0.687} \right) \right| & Re < 1000 \\ 0.44 & Re > 1000 \end{cases}$$

C.2 FLUENT.

C.2.1 O'Rouke and Amsden's Taylor Analogy Breakup model [C-4].

In the Taylor Analogy Breakup model, the equation governing a damped, forced oscillator is

$$F - kx - d\frac{dx}{dt} = m\frac{d^2x}{dt^2} \tag{C-1}$$

where x is the displacement of the droplet equator from its spherical (undisturbed) position. The coefficients of this equation are taken from Taylor's analogy:

$$\frac{F}{m} = C_F \frac{\rho_g u^2}{\rho_l r} \tag{C-2}$$

$$\frac{k}{m} = C_k \frac{\sigma}{\rho_l r^3} \tag{C-3}$$

$$\frac{d}{m} = C_d \frac{\mu_l}{\rho_l r^2} \tag{C-4}$$

where ρ_l and ρ_g are the discrete phase and continuous phase densities, u is the relative velocity of the droplet, r is the undisturbed droplet radius, σ is the droplet surface tension, and μ_l is the droplet viscosity. The dimensionless constants C_F, C_k, and C_d are defined on page C-4.

The droplet is assumed to break up if the distortion grows to a critical ratio of the droplet radius. This breakup requirement is given as

$$x > C_b r \tag{C-5}$$

where C_b is a constant equal to 0.5 if breakup is assumed to occur when the distortion is equal to the droplet radius, i.e., the north and south poles of the droplet meet at the droplet center. This implicitly assumes that the droplet is undergoing only one (fundamental) oscillation mode. Equation C-1 is nondimensionalized by setting $y = x/(C_b r)$ and substituting the relationships in equations C-2 to C-4:

$$\frac{d^2y}{dt^2} = \frac{C_F}{C_b}\frac{\rho_g}{\rho_l}\frac{u^2}{r^2} - \frac{C_k\sigma}{\rho_l r^3}y - \frac{C_d\mu_l}{\rho_l r^2}\frac{dy}{dt} \tag{C-6}$$

where breakup now occurs for $y > 1$. For underdamped droplets, the equation governing y can easily be determined from equation C-6 if the relative velocity is assumed to be constant:

$$y(t) = We_c + e^{-(t/t_d)}\left[\left(y_0 - We_c\right)\cos(\omega\,t) + \frac{1}{\omega}\left(\frac{dy_0}{dt} + \frac{y_0 - We_c}{t_d}\right)\sin(\omega\,t)\right] \tag{C-7}$$

where

$$We = \frac{\rho_g u^2 r}{\sigma} \tag{C-8}$$

$$We_c = \frac{C_F}{C_k C_b}We \tag{C-9}$$

$$y_0 = y(0) \tag{C-10}$$

$$\frac{dy_0}{dt} = \frac{dy}{dt}(0) \tag{C-11}$$

$$\frac{1}{t_d} = \frac{C_d}{2}\frac{\mu_l}{\rho_l r^2} \tag{C-12}$$

$$\omega^2 = C_k\frac{\sigma}{\rho_l r^3} - \frac{1}{t_d^2} \tag{C-13}$$

In equation C-8, u is the relative velocity between the droplet and the gas phase, and We is the droplet Weber number, a dimensionless parameter defined as the ratio of aerodynamic forces to surface tension forces. The droplet oscillation frequency is represented by ω. The constants have been chosen to match experiments and theory [C-4]:

$$C_k = 8$$
$$C_d = 5$$
$$C_F = \frac{1}{3}$$

If equation C-7 is solved for all droplets, those with $y > 1$ are assumed to breakup. The size and velocity of the new child droplets must be determined.

The size of the child droplets is determined by equating the energy of the parent droplet to the combined energy of the child droplets. The energy of the parent droplet is [C-3]

$$E_{\text{parent}} = 4\pi r^2\sigma + K\frac{\pi}{5}\rho_l r^5\left[\left(\frac{dy}{dt}\right)^2 + \omega^2 y^2\right] \tag{C-14}$$

where K is the ratio of the total energy in distortion and oscillation to the energy in the fundamental mode, of the order ~ 0.33. The child droplets are assumed to be nondistorted and nonoscillating. Thus, the energy of the child droplets can be shown to be

$$E_{\text{child}} = 4\pi r^2\sigma\frac{r}{r_{32}} + \frac{\pi}{6}\rho_l r^5\left(\frac{dy}{dt}\right)^2 \tag{C-15}$$

where r_{32} is the Sauter mean radius of the droplet size distribution. r_{32} can be found by equating the energy of the parent and child droplets (i.e., equations C-14 and C-15), setting $y = 1$, and

$$\omega^2 = 8\sigma / \rho_l r^3$$

$$r_{32} = \frac{r}{1 + \frac{8Ky^2}{20} + \frac{\rho_l r^3 (dy/dt)^2}{\sigma}\left(\frac{6K-5}{120}\right)} \tag{C-16}$$

Once the size of the child droplets is determined, the number of child droplets can easily be determined by mass conservation.

FLUENT provides two methods of computing droplet drag coefficient for

- a perfect sphere:

$$C_D = \begin{cases} \left|\frac{24}{Re}\left(1 + \frac{1}{6}\cdot Re^{\frac{2}{3}}\right)\right| & Re < 1000 \\ 0.424 & Re > 1000 \end{cases}$$

- a distorted droplet (also known as dynamic drag):

$$C_D = C_{D,\text{sphere}} (1+2.632.y)$$

The droplet displacement, y, is obtained from equation C-7; therefore, in the limit of no distortion ($y = 0$), the drag coefficient is equivalent to a perfect sphere.

C.3 REFERENCES.

C-1. Reitz, R.D. and Diwakar, R., "Structure of High-Pressure Fuel Spray," SAE Technical Paper Series 870598.

C-2. Pilch, M. and Erdman, C.A., "Use of Breakup Time Data and Velocity History Data to Predict the Maximum Size of Stable Fragments for Acceleration-Induced Breakup of a Liquid Drop," *Int. J. Multiphase Flow*, 13, No. 6, 1987, pp. 741-757.

C-3. Hsiang, L.P. and Faeth, G.M., "Near Limit Drop Deformation and Secondary Breakup," *Int. J. of Multiphase Flow*, 18(5), 1992.

C-4. O'Rouke, P.J. and Amsden, A.A., "The TAB Method for Numerical Calculation of Spray Droplet Breakup," SAE Paper 87-2089, 1987.

APPENDIX D—EFFECTS OF GRID RESOLUTION AND DROPLET RELEASE LOCATION ON DROPLET BREAKUP

D.1 EFFECTS OF GRID RESOLUTION ON DROPLET BREAKUP.

An assessment of the effects of the grid resolution on droplet breakup was conducted with the two-dimensional NACA0012 airfoil shown in figure D-1. The chord length of the airfoil was 20 ft. An O-type mesh was created around the airfoil (figure D-2) with local clustering of grid points near the wall surface to simulate the wall boundary layer. Three computational meshes with grid sizes of 136,000, 200,000, and 300,000 points were generated. A group of single-sized droplets with diameters of 1000 μm were released at about 10 chords upstream of the airfoils, and their initial velocities were set to the flow velocity at the external far-field boundary. The flow field in the computational mesh was computed with the FLUENT code and the following conditions:

- Mach number of 0.3
- Zero angle of attack
- Altitude of 10,000 ft
- k-ε turbulence model
- Pressure far-field boundary

FIGURE D-1. NACA0012 AIRFOIL
(Chord length =20 ft)

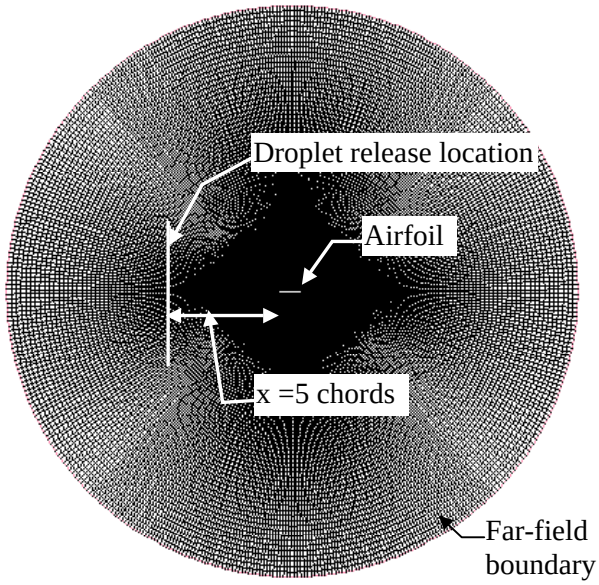

FIGURE D-2. COMPUTATIONAL GRID NEAR THE NACA0012 AIRFOIL

Figures D-3 to D-5 show the characteristics of the breakup process in the computational meshes with 136,000, 200,000, and 300,000 grid points respectively. The assessment of the sensitivity of the grid resolution (on droplet breakup) was based on the breakup behavior and repeatability of the simulated results obtained with each grid.

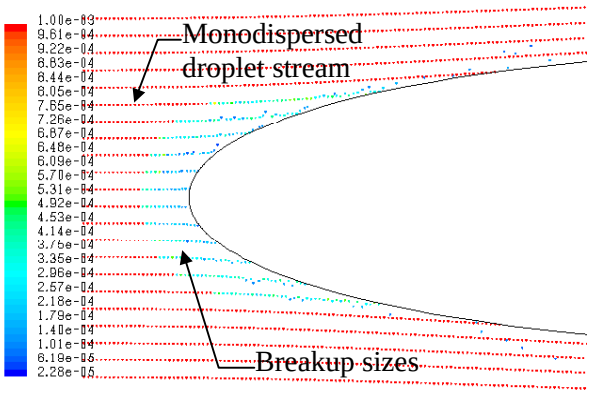

FIGURE D-3. SIMULATED DROPLET BREAKUP WITH 136,000 MESH POINTS

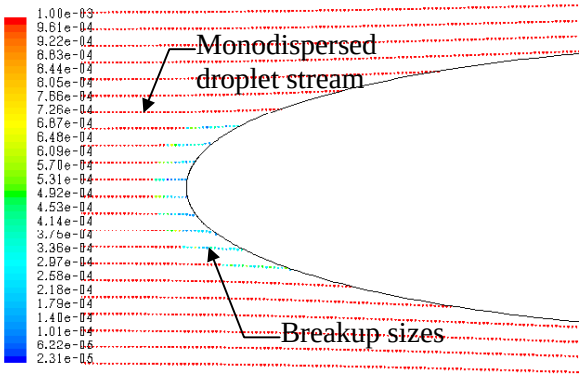

FIGURE D-4. SIMULATED DROPLET BREAKUP WITH 200,000 MESH POINTS

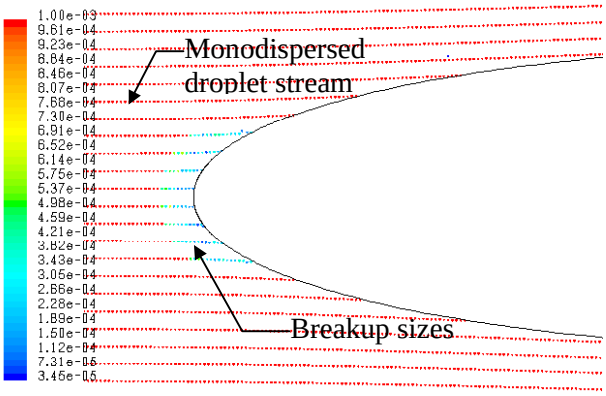

Effects of Grid Resolution on Breakup

NACA 0012 Airfoil
Chord = 240 inches
Droplet diameter = 1000 μm
Droplet release distance = 10 chord
Droplet release velocity = free-stream velocity
Time step size = 1e-4 s

FIGURE D-5. SIMULATED DROPLET BREAKUP WITH 300,000 MESH POINTS

The results in figures D-3 to D-5 show that the breakup characteristics obtained with the coarser mesh (136,000 grid points) are different to those computed with the finer meshes (200,000 and 300,000 grid points). A greater number of droplet breakups were found in the mesh with 136,000 grid points (figure D-3) compared to those simulated in the meshes with 200,000 or 300,000 grid points (figures D-4 and D-5 respectively). Droplet breakup also occurred (relatively) further upstream and extended further aft (of the airfoil leading edge) in the coarser mesh case. The breakup process in the finer meshes exhibited greater consistency and repeatability, which was probably due to the more accurate pressure gradients predicted with the finer meshes.

D.2 EFFECTS OF DROPLET RELEASE LOCATION ON DROPLET BREAKUP.

The effect of the droplet release location was also investigated by selecting release locations at 3, 4, 5, 6, and 10 chords upstream of the airfoil. This was performed using the computational mesh with 300,000 grid points. The results of this analysis are shown in figures D-6a to D-6e for droplet release locations at a 3- to 10-chord distance.

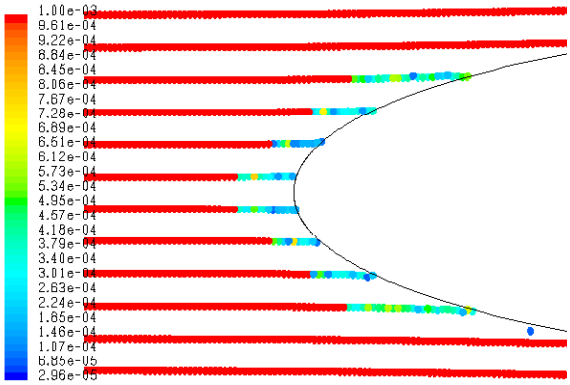

FIGURE D-6a. SIMULATED DROPLET BREAKUP WITH THE RELEASE LOCATION AT A 3-CHORD DISTANCE

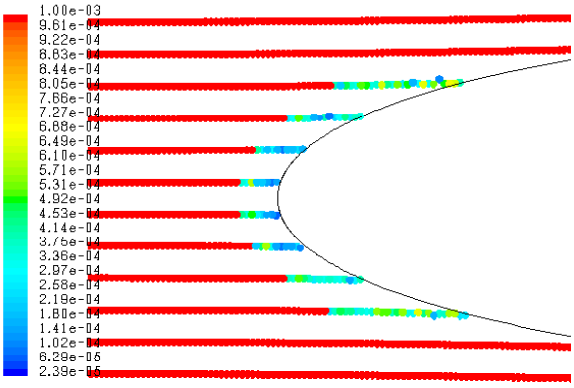

FIGURE D-6b. SIMULATED DROPLET BREAKUP WITH THE RELEASE LOCATION AT A 4-CHORD DISTANCE

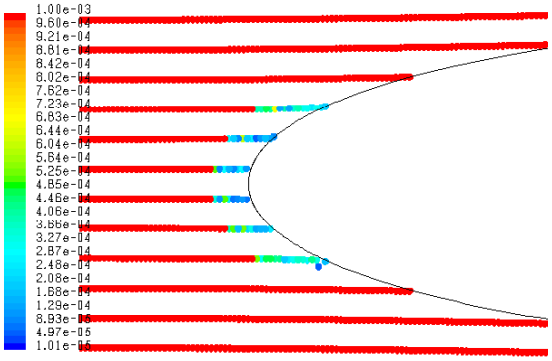

FIGURE D-6c. SIMULATED DROPLET BREAKUP WITH THE RELEASE LOCATION AT A 5-CHORD DISTANCE

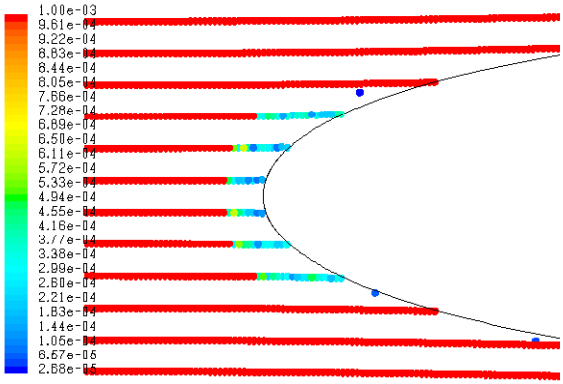

FIGURE D-6d. SIMULATED DROPLET BREAKUP WITH THE RELEASE LOCATION AT A 6-CHORD DISTANCE

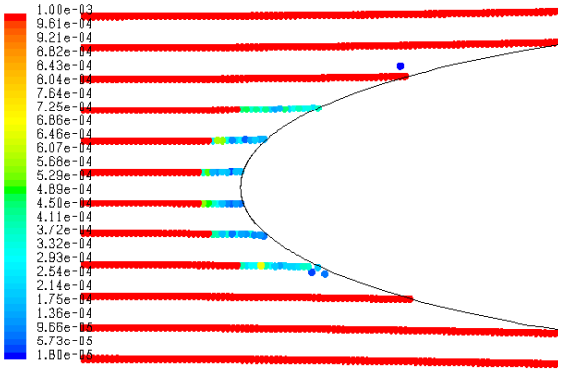

<u>Effects of Droplet Release Location on Breakup</u>

NACA 0012 Airfoil
Chord = 240 inches
Droplet diameter = 1000 μm
Mesh size = 300,000 points
Droplet release velocity = free-stream velocity
Time step size = 1e-4 s

FIGURE D-6e. SIMULATED DROPLET BREAKUP WITH THE RELEASE LOCATION AT A 10-CHORD DISTANCE

The simulations for droplets released at a 3- and 4-chord distance, figures D-6a and D-6b respectively, exhibited more breakups that extended further aft of the LE of the airfoil. For droplet release at locations greater than 4 chords from the airfoil, the breakup process exhibited greater consistency and repeatability, as shown in figures D-6b to D-6e. It is believed that the droplet relaxation time (i.e., the time required for a droplet to reach the free-stream velocity) was the main cause of this effect. Large droplets require longer relaxation times (hence, longer distances) to reach local free-stream velocity due to their greater inertias.

Figure D-7 shows the variation of the free-stream velocity with (upstream) distance from the airfoil. Also shown in the figure are the droplet release locations. The curve shows that droplets released at 3- and 4-chords upstream of the airfoil coincided with regions of low-velocity gradient. Since the initial droplet velocity at these two locations was set equal to the air velocity near the far-field computational boundary (to represent a suspended droplet), a small relative droplet-air velocity existed at the release locations that might have caused premature droplet breakup. However, as the droplet release location was moved further upstream (i.e., greater than 4-chord lengths), the initial relative velocity was smaller; hence, it had a lesser effect on breakup.

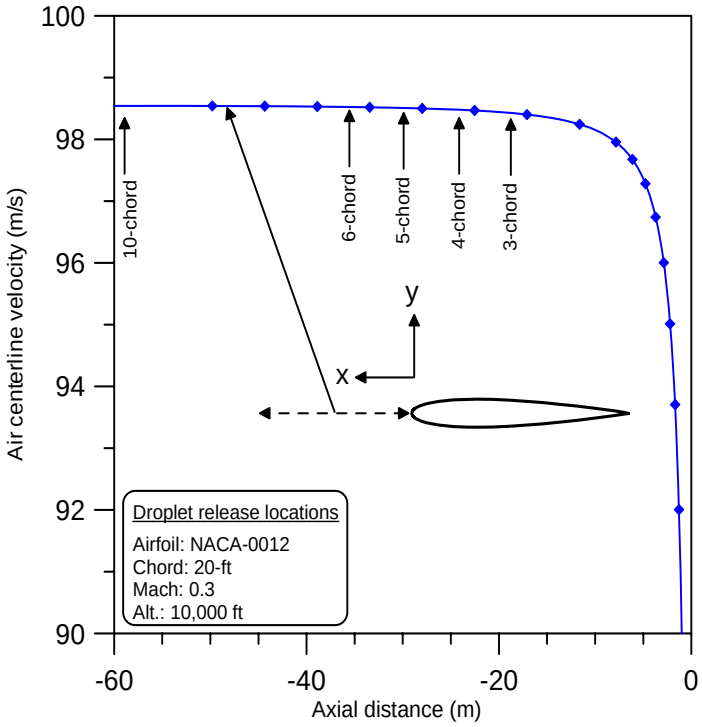

FIGURE D-7. DROPLET RELEASE LOCATIONS AND CENTERLINE AIR VELOCITY

The investigations into the effect of the grid resolution and initial droplet release location on the breakup process suggested that the computational mesh appropriate for the current study should not be less than 200,000 points, and droplet release location should be at least 5 chords away from the airfoil.

APPENDIX E—VELOCITY DISTRIBUTION IN A VERTICAL TUNNEL

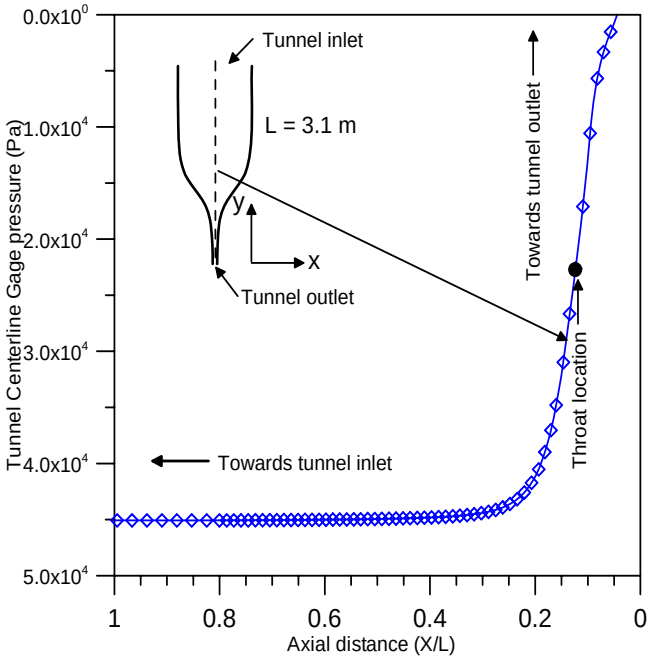

FIGURE E-1. TUNNEL CENTERLINE VELOCITY DISTRIBUTION USED FOR DROPLET BREAKUP STUDIES (KENNEDY [E-1])

REFERENCES.

E-1. Kennedy, J.B. and Roberts, J., “Rain Ingestion in a Gas Turbine Engine,” ILASS-AMERICAS, Inst. of Liquid Atomization and Spray Systems, 4th Annual Conference, Hartford, CT, USA, 1990, pp. 154-186.